NAVAL POSTGRADUATE SCHOOL

MONTEREY, CALIFORNIA

THESIS

ROBUSTNESS OF CONTROL LAWS IMPLEMENTED IN VISUAL BASED TARGET TRACKING SYSTEM

by

Lee Han Chuan

December 2009

Thesis Advisor: Issac I. Kaminer
Co-Advisor: Vladimir N. Dobrokhodov

Approved for public release; distribution is unlimited

REPORT DOCUMENTATION PAGE			Form Approved OMB No. 0704-0188
Public reporting burden for this collection of information is estimated to average 1 hour per response, including the time for reviewing instruction, searching existing data sources, gathering and maintaining the data needed, and completing and reviewing the collection of information. Send comments regarding this burden estimate or any other aspect of this collection of information, including suggestions for reducing this burden, to Washington headquarters Services, Directorate for Information Operations and Reports, 1215 Jefferson Davis Highway, Suite 1204, Arlington, VA 22202-4302, and to the Office of Management and Budget, Paperwork Reduction Project (0704-0188) Washington DC 20503.			
1. AGENCY USE ONLY ***(Leave blank)***	**2. REPORT DATE** December 2009	**3. REPORT TYPE AND DATES COVERED** Master's Thesis	
4. TITLE AND SUBTITLE: Robustness of Control Laws Implemented in Visual Based Tracking System		**5. FUNDING NUMBERS**	
6. AUTHOR(S) Lee Han Chuan			
7. PERFORMING ORGANIZATION NAME(S) AND ADDRESS(ES) Naval Postgraduate School Monterey, CA 93943-5000		**8. PERFORMING ORGANIZATION REPORT NUMBER**	
9. SPONSORING / MONITORING AGENCY NAME(S) AND ADDRESS(ES) N/A		**10. SPONSORING / MONITORING AGENCY REPORT NUMBER**	
11. SUPPLEMENTARY NOTES The views expressed in this thesis are those of the author and do not reflect the official policy or position of the Department of Defense or the U.S. Government.			
12a. DISTRIBUTION / AVAILABILITY STATEMENT Approved for public release; distribution is unlimited		**12b. DISTRIBUTION CODE**	

13. ABSTRACT

The previously developed guidance law implemented onboard the Small Unmanned Aerial Vehicle (SUAV) relies exclusively on the information from the image processing software and allows to perform coordinated SUAV guidance and vision based target tracking and motion estimation. This enables "passive only" coordinated tracking of non-cooperative targets. An analysis of the system performance shows that the developed target tracking law demonstrates poor range holding capability when the target performs evasive maneuvers. Therefore a new guidance law has been formulated by resolving SUAV dynamics with respect to the moving target frame as oppose to the inertial frame in previous formulation. This simple modification results in theoretically achievable perfect range holding capability for the price of requiring the target motion information to be known. As a result, this new modification is based on the assumption of known target states which in turn requires an implementation of a target motion estimator. An obvious tradeoff in performance of the "passive only" and "estimator based" target tracking systems is investigated in this thesis under the realistic conditions including target loss events.

This work extends previous results by investigating the performance of both guidance laws to the variation in target velocity and frequency of tracking loss events. The results obtained are based on the high fidelity 6DOF simulation implemented in SIMULINK, and analyzed using the multi-criteria optimization methodology introduced in the previous work. The results show that both guidance laws suffer predictable degradation in performance when subject to the external disturbances and tracking loss events. However, in the absence of tracking loss events, the new guidance law suffers less degradation in performance as compared to the old guidance law. When "frequency" of tracking loss events is low (less than 12%), the new guidance law is still able to provide better performance than the old guidance law As the "frequency" of tracking loss events increases further (between 12% to 25%), the performance of the new guidance law starts rapidly degrading converging to that of the initial system; as the target estimator is no longer able to provide a good prediction of the target velocity and heading to the guidance law.

14. SUBJECT TERMS Unmanned Aerial Vehicle, UAV, Autonomous Guidance, Target Tracking, Control, Visual Based Target Tracking, Simulink, Hardware in the loop, Piccolo, xPC Target, PC-104			**15. NUMBER OF PAGES** 81 / **16. PRICE CODE**
17. SECURITY CLASSIFICATION OF REPORT Unclassified	**18. SECURITY CLASSIFICATION OF THIS PAGE** Unclassified	**19. SECURITY CLASSIFICATION OF ABSTRACT** Unclassified	**20. LIMITATION OF ABSTRACT** UU

NSN 7540-01-280-5500 Standard Form 298 (Rev. 2-89)

THIS PAGE INTENTIONALLY LEFT BLANK

Approved for public release; distribution is unlimited

ROBUSTNESS OF CONTROL LAWS IMPLEMENTED IN VISUAL BASED TARGET TRACKING SYSTEM

Han Chuan, Lee
Civilian, Defence Science & Technology Agency
M.S. (Electrical Engineering), National University of Singapore, 2005

Submitted in partial fulfillment of the
requirements for the degree of

MASTER OF SCIENCE IN ENGINEERING SCIENCE
(MECHANICAL ENGINEERING)

from the

NAVAL POSTGRADUATE SCHOOL
December 2009

Author: Lee Han Chuan

Approved by: Professor Issac I. Kaminer
Thesis Advisor

Professor Vladimir N. Dobrokhodov
Co Advisor

Professor Knox T. Millsaps
Chairman, Department of Mechanical and Astronautical Engineering

THIS PAGE INTENTIONALLY LEFT BLANK

ABSTRACT

The previously developed guidance law implemented onboard the Small Unmanned Aerial Vehicle (SUAV) relies exclusively on the information from the image processing software and allows the performance of coordinated SUAV guidance and vision-based target tracking and motion estimation. This enables “passive only” coordinated tracking of non-cooperative targets. An analysis of the system performance shows that the developed target tracking law demonstrates poor range holding capability when the target performs evasive maneuvers. Therefore, a new guidance law has been formulated by resolving SUAV dynamics with respect to the moving target frame, as opposed to the inertial frame in previous formulation. This simple modification results in theoretically achievable perfect range holding capability for the price of requiring the target motion information to be known. As a result, this new modification is based on the assumption of known target states, which in turn requires an implementation of a target motion estimator. An obvious tradeoff in performance of the “passive only” and “estimator based” target tracking systems is investigated in this thesis under realistic conditions including target loss events.

This work extends previous results by investigating the performance of both guidance laws to the variation in target velocity and frequency of tracking loss events. The results obtained are based on the high fidelity 6DOF simulation implemented in SIMULINK, and analyzed using the multi-criteria optimization methodology introduced in the previous work. The results show that both guidance laws suffer predictable degradation in performance when subject to the external disturbances and tracking loss events. However, in the absence of tracking loss events, the new guidance law suffers less degradation in performance as compared to the old guidance law. When “frequency” of tracking loss events is low (less than 12%), the new guidance law is still able to provide better performance than the old guidance law As the “frequency” of tracking loss events increases further (between 12% to 25%), the performance of the new guidance law starts rapidly degrading, converging to that of the initial system; the target estimator is no longer able to provide a good prediction of the target velocity and heading to the guidance law.

THIS PAGE INTENTIONALLY LEFT BLANK

TABLE OF CONTENTS

LIST OF FIGURES

THIS PAGE INTENTIONALLY LEFT BLANK

LIST OF TABLES

THIS PAGE INTENTIONALLY LEFT BLANK

ACKNOWLEDGMENTS

The author is grateful to his two thesis advisors for imparting their knowledge and research experience, and making the entire project an interesting learning experience. First and foremost, the author would like to thank Professor Isaac Kaminer for providing the opportunity to work on this interesting project, and for all his guidance throughout the project.

Secondly, the author would like to thank Professor Vladimir Dobrokhodov for all his valuable help and patience in explaining the difficult concepts contained in the thesis. He has provided invaluable guidance on the development and implementation of the modifications to the Visual Based Target Tracking (VBTT) system.

Lastly, the author would like to thank his wife for her support and encouragement during the course of his studies at the Naval Postgraduate School.

THIS PAGE INTENTIONALLY LEFT BLANK

I. INTRODUCTION

A. BACKGROUND

Network Centric Warfare (NCW) is the best term developed to date to describe the way the modern military forces will fight in the coming Information Age. It is defined as an information superiority-enabled concept of operations that generates increased combat power by networking sensors, decision makers, and shooters to achieve shared awareness, increased speed of command, higher tempo of operations, greater lethality, increased survivability, and a degree of self-synchronization. Essentially, NCW translates information superiority into combat power by effectively linking knowledgeable entitles in the battle-space [1].

The Unmanned Aerial Vehicle (UAV) plays an important role in NCW and is increasingly used by many military forces around the world to perform primarily Intelligence, Surveillance and Reconnaissance (ISR), communication relaying and small payload delivery missions in modern day's battlefield. For instance, the U.S military had reported that an increased usage in UAVs was observed in the wars in Iraq and Afghanistan[1]. Faced with the ever growing demand to deliver real-time information to other entitles in the battle-space, the UAV operators will have to multi-task and work harder in order to effectively control the UAV and process key intelligence.

The current process for visually tracking a target with a pan-tilt gimballed camera mounted on a UAV requires two operators. The first operator is responsible for controlling the platform (UAV) while the second operator controls the payload (orientation of the gimballed camera). In order to keep the camera aimed at the target, the two UAV operators have to coordinate closely and continuously communicate with each other. If the target makes an evasive manoeuvre and gets out of the gimbal operational limit or out of the camera resolution range, the payload operator will need the UAV pilot to manoeuvre the platform in order to reacquire the target again. This can take a

[1] Armed Forces International, "US Military's UAV Missions Increasing." [Accessed November 09] Available: http://www.armedforces-int.com/news/us-militarys-uav-missions-increasing.html

significant amount of time even if both operators are very well trained. Obviously, a fully autonomous UAV equipped with the proper instrumentation and control software would help to alleviate the problem of human constraints. A Visual Based Target Tracking (VBTT) system that automatically couples the dual objective of manoeuvring the unmanned aerial platform and its sensor payload should significantly support both operators, enabling them to for mode challenging missions than ever before.

B. OVERVIEW OF RESEARCH PROJECT

This thesis is an ongoing effort within the Unmanned Systems Research Group in the Naval Postgraduate School (NPS) to develop a prototype VBTT system for a SUAV, as shown in Figure 1.

Figure 1. NPS Small UAV (Sig Rascal)

The VBTT system comprises the modified remotely controlled small aircraft equipped with an industrial autopilot and a miniature pan-tilt gimbaled camera using commercial off the shelf components and custom build control software. The system controls both the platform and the gimbaled camera with the objective to (i) keep the operator-selected target in the center of the video image, to (ii) coordinate guidance of the UAV around the target, and to (iii) provide a real time estimate of the target motion including its geodetic position, speed and heading.

Three major components were developed and integrated onboard to create the VBTT system [9]. The first component of the system includes a VBTT capability that uses the video imagery provided by the gimbaled camera. Development of this component involves the design of a miniaturized gimbaled camera and a controller, and

integration of the automated motion tracking software by PercepiVU, Inc [2]. The development of the adaptive controller for the gimbaled camera loop is presented in Section III. The second component consists of a target motion estimator and the development for the estimator is also presented in Section III.

The final component of the system includes the guidance law for the SUAV. The control algorithm is designed to navigate the SUAV around the target while keeping the target in the center of the camera frame. The range estimation error is at its minimum when the target is moving in parallel with the camera image plane [9].

C. OBJECTIVES AND SCOPE OF WORK

This thesis extends previous works [2] – [5] by investigating the robustness of the newly developed control law in response to variation in target velocity and "frequency" of tracking loss events. The results obtained are to be based on the high fidelity 6DOF simulations implemented in SIMULINK and analyzed using the multi-criteria optimization technique introduced in previous work [10]. The results obtained are then compared against those that are obtained from the current control law.

THIS PAGE INTENTIONALLY LEFT BLANK

II. DEVELOPMENT OF CONTROL LAW

A. COORDINATE SYSTEMS

Multiple coordinate frames are often used to define the motions or behaviors of various objects in complex dynamic systems. The translational and rotational kinematics states (i.e. the positions, velocities and accelerations) of an object can be fully described in any frame as long as the transformation relationships between the coordinate frames are known. The following coordinate systems were used in the development of the control laws in this thesis [2] – [10].

1. Navigation Inertia Coordinate Frame (I – Frame)

This local level frame assumed a flat earth model in the vicinity of the reference navigation point; the X_n – Y_n axes lie in a plane tangent to the reference point origin on the earth ellipsoid surface, and the Z_n axis lie perpendicular to that ellipsoid surface. As illustrated in Figure 2, this is a North-East-Down (NED) coordinate system and is also known as the Local Tangent Plane (LTP).

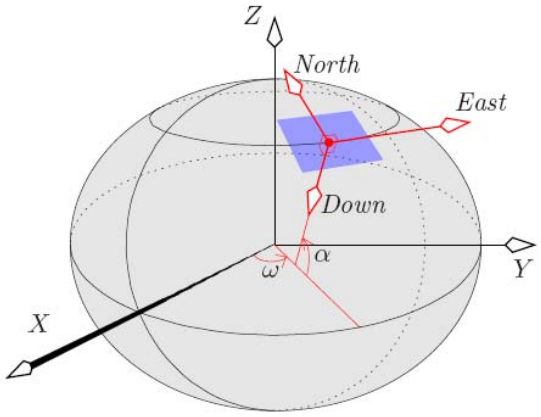

Figure 2. NED Coordinate System

2. SUAV Body Coordinate Frame (B – Frame)

A convenient coordinate system for developing the equations of motion of the SUAV is a right-hand orthogonal system with its origin centered at the aircraft's center of gravity. Conventionally, the x-axis points forward along the longitudinal axis of the aircraft, the y-axis points outward towards the right wing, and the z-axis points downward from the origin (see Figure 3).

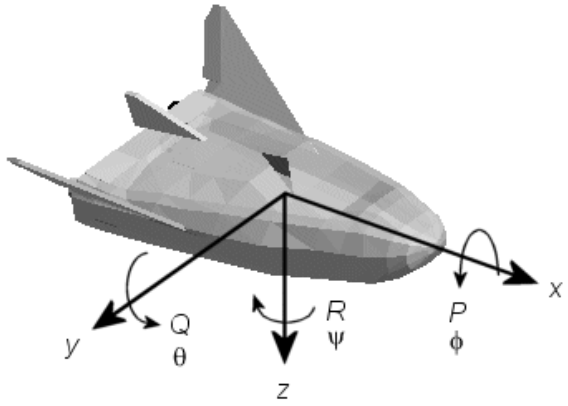

Figure 3. SUAV Body Coordinate Frame

3. Gimbal Platform Coordinate Frame (G – Frame)

The gimbal coordinate frame is a right-hand orthogonal coordinate system whose origin is at the location of the camera mount. The x-axis of the gimbal frame points forward along the longitudinal axis of the gimbal platform, the y-axis points outward towards the right-hand side, and the z-axis points downward from the origin.

4. Image Plane Coordinate Frame (P – Frame)

The image plane reference frame is the coordinate system used to describe the location of the target in the image plane. It is a two-dimensional coordinate system with the u-axis aligned with the y-axis of the camera coordinate frame, and the v-axis aligned with the negative z-axis of the camera coordinate frame.

B. EULER ANGLES

Euler angles are the classical means of representing rotations in three-dimensional Euclidean space. The triplet of Euler angles (ϕ, θ, ψ) relates two orthogonal coordinate systems having a common origin and the coordinate frames can be transformed from one to the other through a series of rotations defined by the Euler angles. Conventionally, when the Euler angles used to describe the orientation of the aircraft body in relation to the inertia coordinate frame, these Euler angles are known as roll, pitch and yaw [6] – [8].

C. RELATIONSHIPS BETWEEN COORDINATE SYSTEMS

A coordinate transformation is a conversion from one coordinate system to another, to describe the same space. A rotation is a type of transformation from one system of coordinates to another such the distance between any two points remains invariant under the transformation. A rigid body in space can be represented by a [3 x 1] vector, and its orientation to its own current coordinate frame or a transformed coordinate frame can be uniquely described by a [3 x 3] rotation matrix at any instant in time [6] – [7].

1. Rotation Matrices

The rotation matrices for a single two-dimensional rotation about each individual axis are given below. The angle of rotation is the Euler angle that corresponds to each individual axis.

$$R_z(\psi) = \begin{bmatrix} \cos(\psi) & \sin(\psi) & 0 \\ -\sin(\psi) & \cos(\psi) & 0 \\ 0 & 0 & 1 \end{bmatrix} \tag{1}$$

$$R_Y(\theta) = \begin{bmatrix} \cos(\theta) & 0 & -\sin(\theta) \\ 0 & 1 & 0 \\ \sin(\theta) & 0 & \cos(\theta) \end{bmatrix} \tag{2}$$

$$R_X(\phi) = \begin{bmatrix} 1 & 0 & 0 \\ 0 & \cos(\phi) & \sin(\phi) \\ 0 & -\sin(\phi) & \cos(\phi) \end{bmatrix} \quad (3)$$

The complete rotation or transformation of the coordinate system is the sequential combination of the two dimensional rotations about each axis. The sequence, or order of the rotation, is necessary to properly define the orientation of the body and to preserve the orthogonality conditions (right-hand system or left-hand system) of the transformed axes.

2. Coordinates Transformation

The coordinate transformation, or rotation from the inertia frame to the camera frame, can be obtained via sequential coordinate transformations from one frame to the other in the correct logical order, as shown below:

$${}^{C}_{I}R = {}^{C}_{G}R\,{}^{G}_{B}R\,{}^{B}_{I}R \quad (4)$$

where ${}^{B}_{I}R$ = coordinate rotation from inertia frame to body frame

${}^{G}_{B}R$ = coordinate rotation from body frame to gimbal frame

${}^{C}_{G}R$ = coordinate rotation from gimbal frame to camera frame

a. Inertial Frame to Body Frame Transformation

The coordinate transformation from the inertia frame to the body frame is simply the product of the three individual rotation matrices:

$${}^{B}_{I}R = R_X\left({}^{I}\phi_B\right) R_Y\left({}^{I}\theta_B\right) R_Z\left({}^{I}\psi_B\right) \quad (5)$$

b. Body Frame to Gimbal Frame Transformation

The coordinate transformation from the body frame to the gimbal frame only involves rotation through two angles because the gimbal platform is a two axis coordinate system. As there is no rotation along the x-axis (roll rotation), the gimbal roll angle is taken to be zero.

$${}^{G}_{B}R = R_Y\left({}^{B}\theta_G\right) R_Z\left({}^{B}\psi_G\right) \quad (6)$$

c. Gimbal Frame to Camera Frame Transformation

The coordinate transformation between the gimbal frame and the camera frame allows for compensation of any misalignment angles that exist between the mounting of the camera platform with the gimbal platform. In all likelihood, some or all of the rotation angles will be zero because the axes will be directly aligned.

$$ {}^{C}_{G}R = R_x\left({}^{G}\phi_C\right)R_Y\left({}^{G}\theta_C\right)R_Z\left({}^{G}\psi_C\right) \tag{7} $$

d. Camera Frame to Image Plane Frame Transformation

The coordinate transformation between the camera frame and the image plane frame is not a rotational but a positional transformation. As illustrated by Figure 4, the position of an object in the image plane frame from a position in the camera frame is given as below:

$$ \begin{bmatrix} P_U \\ P_V \end{bmatrix} = \frac{f}{c_x}\begin{bmatrix} c_y \\ -c_z \end{bmatrix} \tag{8} $$

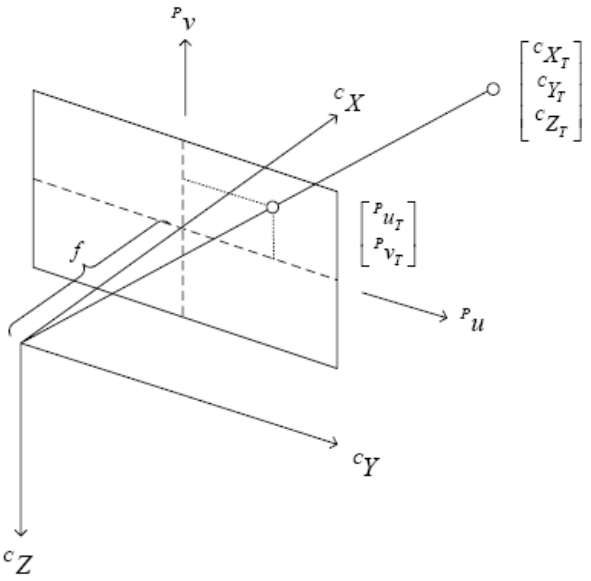

Figure 4. Image Plane Reference Frame

It is of interest to note that, unlike the previous rotational transformations, the camera to image plane transformation is irreversible. This is due to the transformation of a three-dimensional coordinate system to a two-dimensional coordinate system.

3. Angular Velocities Transformation

a. Body Frame Angular Velocities with Respect to Inertial Frame

The angular velocity vector, ω, in the body fixed coordinate system of the SUAV, has components [p, q, r] in the x, y and direction respectively. The resulting relationships with the Euler angle rates $[\dot{\phi}_B, \dot{\theta}_B, \dot{\psi}_B]$ for which are stated as follows:

$$ {}^{B}\omega_{BI} = R_X\left({}^{I}\phi_B\right)R_Y\left({}^{I}\theta_B\right)R_Z\left({}^{I}\psi_B\right)\begin{bmatrix}0\\0\\\dot{\psi}_B\end{bmatrix} + R_X\left({}^{I}\phi_B\right)R_Y\left({}^{I}\theta_B\right)\begin{bmatrix}0\\\dot{\theta}_B\\0\end{bmatrix} + R_X\left({}^{I}\phi_B\right)\begin{bmatrix}\dot{\phi}_B\\0\\0\end{bmatrix} $$

$$ {}^{B}\omega_{BI} = \begin{bmatrix}\omega_x\\\omega_y\\\omega_z\end{bmatrix} = \begin{bmatrix}p_B\\p\\\omega_z\end{bmatrix} = \begin{bmatrix}\dot{\psi}_x + \dot{\theta}_x + \dot{\phi}_x\\\dot{\psi}_y + \dot{\theta}_y + \dot{\phi}_y\\\dot{\psi}_z + \dot{\theta}_z + \dot{\phi}_z\end{bmatrix} = \begin{bmatrix}\dot{\phi}_B - \dot{\psi}_B \sin^I \theta_B\\\dot{\psi}_B \cos^I \theta_B \sin^I \phi_B + \dot{\theta}_B \cos^I \phi_B\\\dot{\psi}_B \cos^I \theta_B \sin^I \phi_B - \dot{\theta}_B \cos^I \phi_B\end{bmatrix} \quad (9) $$

Expressing $[\dot{\phi}_B, \dot{\theta}_B, \dot{\psi}_B]$ in terms of $[p_B, q_B, r_B]$ below, we observe the singularity problem in Equation (10) when ${}^{I}\theta_B = \pm 90°$:

$$ \begin{bmatrix}\dot{\psi}_B\\\dot{\theta}_B\\\dot{\phi}_B\end{bmatrix} = \begin{bmatrix}\frac{1}{\cos\left({}^{I}\theta_B\right)}\left[q_B \sin\left({}^{I}\phi_B\right) + r_B \cos\left({}^{I}\phi_B\right)\right]\\q_B \cos\left({}^{I}\phi_B\right) - r_B \sin\left({}^{I}\phi_B\right)\\p_B + \tan\left({}^{I}\theta_B\right)\left[q_B \sin\left({}^{I}\phi_B\right) + r_B \cos\left({}^{I}\phi_B\right)\right]\end{bmatrix} \quad (10) $$

b. Gimbal Frame Angular Velocities with Respect to Inertial Frame

The angular velocities of the gimbal frame with respect to the inertia frame are as shown below. Equation (10) relates the angular velocity expressed in the gimbal platform frame while Equation (11) describes the transformation of the same angular rate in the inertia frame.

$$^{G}\omega_{GI} \triangleq R_Y\left(^{I}\theta_G\right)R_Z\left(^{I}\psi_G\right)\begin{bmatrix} p_B \\ q_B \\ r_B \end{bmatrix} + R_Y\left(^{I}\theta_G\right)R_Z\left(^{I}\psi_G\right)\begin{bmatrix} 0 \\ 0 \\ \dot{\psi}_G \end{bmatrix} + R_y\left(^{I}\theta_G\right)\begin{bmatrix} 0 \\ \dot{\theta}_G \\ 0 \end{bmatrix}$$

$$^{G}\omega_{GI} = {}^{G}_{B}R\begin{bmatrix} p_B \\ q_B \\ r_B \end{bmatrix} + {}^{G}_{B}R\begin{bmatrix} 0 \\ 0 \\ \dot{\psi}_G \end{bmatrix} + R_y\left(^{I}\theta_G\right)\begin{bmatrix} 0 \\ \dot{\theta}_G \\ 0 \end{bmatrix} \tag{11}$$

$$^{I}\omega_{GI} = {}^{I}_{G}R\,{}^{G}\omega_{GI} = {}^{I}_{G}R\begin{bmatrix} p_G \\ q_G \\ r_G \end{bmatrix} \tag{12}$$

c. Camera Frame Angular Velocities with Respect to Inertia Frame

If the camera frame is perfectly aligned with the gimbal frame, there will not be any rotation between the two frames. Hence, the angular rates between the two frames will be the same. The relationships are expressed as below:

$$^{C}\omega_{CI} = {}^{C}_{G}R\,{}^{G}\omega_{GI}$$

Since ${}^{C}_{G}R = I$,

$$^{C}\omega_{CI} = {}^{G}\omega_{GI} = \begin{bmatrix} p_G \\ q_G \\ r_G \end{bmatrix} \tag{13}$$

$$^{I}\omega_{CI} = {}^{I}\omega_{GI} \tag{14}$$

D. KINEMATIC EQUATIONS OF SUAV-TARGET MOTION

A simplified two dimensional kinematics model is presented in Figure 7. The figure depicts the kinematic relationships between the angles used to characterize the relative motion of the SUAV-Target system. In order to simplify the formulation of the target tracking and UAV control tasks to a 2D plane, it is assume that the autopilot is capable of maintaining level flight of the UAV and the onboard two-axis gimbal is inertially stabilized [3], [5], [9], [10].

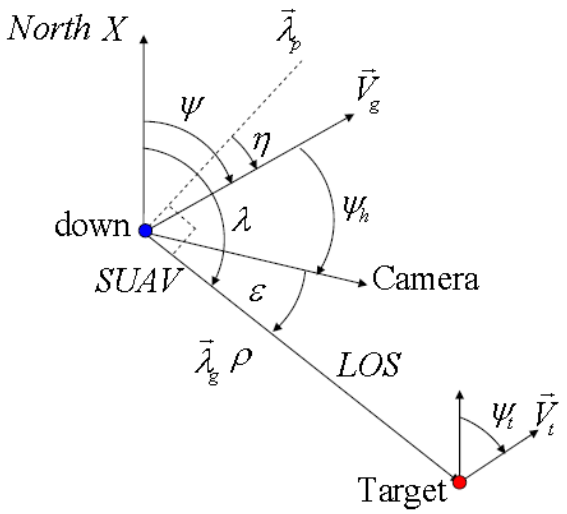

η	= Navigation Error	ψ	= UAV Heading in Inertia Frame
ε	= Camera LOS Pan Error	ψ_t	= Target Heading in Inertia Frame
λ	= LOS Angle in Inertia Frame	ψ_h	= Camera Angle in UAV Body Frame
$\vec{\lambda}_g$	= LOS Vector	$\overrightarrow{V_g}$	= SUAV Ground Speed in Inertia Frame
$\overrightarrow{\lambda_p}$	= Normal to LOS Vector	$\vec{V}_t$	= Target Ground Speed in Inertia Speed

Figure 5. Kinematics of SUAV – Target Motion

The following set of basic kinematical relations is derived directly from the kinematics of Figure 5. First, it is observed that:

$$\eta = \psi - \left(\lambda - \frac{\pi}{2} \right) \tag{15}$$

Next, projecting the SUAV and target speed vectors onto the LOS results in the time derivative of the horizontal range to the target:

$$\dot{\rho}_e = -V_g \sin\eta + V_t \sin\left(\psi_t - \left(\psi - \eta\right)\right) \tag{16}$$

Similarly, projecting the same vectors onto the line orthogonal to the LOS produces the rotation speed of the LOS:

$$\dot{\lambda} = \frac{V_g \cos\eta}{\rho} - \frac{V_t \cos\left(\psi_t - \left(\psi - \eta\right)\right)}{\rho} \tag{17}$$

Finally, an expression for the tracking error ε is given by:

$$\varepsilon = \lambda - \psi - \psi_h \tag{18}$$

Substituting Equation 17 into time derivatives of Equations 15 and 18 produces the following set of equations describing the kinematics of the tracking problem:

$$\dot{\eta} = -\frac{V_g \cos\eta - V_t \cos\left(\psi_t - \left(\psi - \eta\right)\right)}{\rho} + \dot{\psi} \tag{19a}$$

$$\dot{\rho}_e = -V_g \sin\eta + V_t \sin\left(\psi_t - \left(\psi - \eta\right)\right) \tag{19b}$$

$$\dot{\varepsilon} = \frac{V_g \cos\eta - V_t \cos\left(\psi_t - \left(\psi - \eta\right)\right)}{\rho} - \dot{\psi} - \dot{\psi}_h \tag{19c}$$

E. CONTROL LAW DESIGN

1. Initial Control Law Designs

The initial control law design of the VBTT system has the following form [2]:

$$\dot{\psi} = sign\left(Bias - k_1\eta\right) \tag{20a}$$

$$\dot{\psi}_h = k_2\varepsilon \tag{20b}$$

The advantage of this control law is that it is simple to implement and the algorithm relies exclusively on the information gathered from the image processing software. However, two main limitations are observed for this control law. Firstly, as a fixed bias value is applied to turn the SUAV in Equation (20a), this results in a slow converging speed to any other desired range commanded, except to the desired range that corresponds to the arbitrary turning bias value. Secondly, as the camera LOS turn rate is independent of the SUAV turn rate, this results in poor control of the camera LOS and a large k_2 value is needed to keep the camera LOS closely aligned to the SUAV-target LOS.

To overcome these limitations, the control law is then adjusted to the following form [3]:

$$\dot{\psi} = \frac{\vec{V}_g}{\rho_d}\cos\eta - k_1\eta \tag{21a}$$

$$\dot{\psi}_h = k_1\eta + k_2\varepsilon \tag{21b}$$

With the addition of a $k_1\eta$ term to Equation (20b), the camera control has become more efficient as the camera turn rate is now coupled to the SUAV turn rate. The turning bias in Equation (20a) is replaced with the dynamically adjusted quantity in Equation (21a), which varies with the SUAV ground speed and the desired range to target. For a stationary target, if the SUAV starts tracking a target at a distance smaller than the commanded range, it will spiral outwards to the desired range. Conversely, if the SUAV starts tracking a target at a distance larger than the commanded range, it will spiral inwards to the desired range. The navigation angle error η will approach to zero when the SUAV establishes a circular orbit about a stationary target at the desired range.

The feedback system consisting of Equations (19) and (21) is given by:

$$\dot{\eta} = -V_g\rho_e\cos\eta - k_1\eta + V_t\cos(\eta - \psi)\bar{\rho} \tag{22a}$$

$$\dot{\rho}_e = \bar{\rho}^2 V_g\sin\eta - V_t\sin(\eta - \psi)\bar{\rho}^2 \tag{22b}$$

$$\dot{\varepsilon} = V_g\rho_e\cos\eta - k_2\varepsilon - V_t\cos(\eta - \psi)\bar{\rho} \tag{22c}$$

where $\rho_e = \frac{1}{\rho} - \frac{1}{\rho_d}$; $\quad \dot{\rho}_e = -\frac{1}{\rho^2}\dot{\rho}$; $\quad \bar{\rho} = \rho_e + \frac{1}{\rho_d}$

This control law is currently being used in the VBTT system for the NPS SUAV. For convenience of notation, this control law will be referred to as the "current control law". Notice that the current control law still relies exclusively on the information gathered from the image processing software.

2. New Control Law Design

From Equation (22b), it is observed that when the navigation error η is driven to zero, $\dot{\rho}_e = V_t\sin(\psi)\bar{\rho}^2 \neq 0$ (unless the target is stationary). Hence, the objective of the

current control law to regulate η to zero will not result in a constant ρ. This results in the need to reformulate the control objective and to come out with a new control law design [5].

According to Equations (19a) and (19b), the kinematics for η and ρ is independent of the camera LOS pan error ε. Thus, in the design of the new control law, it is assumed that ε is in the visible angle range to provide the necessary visual feedback.

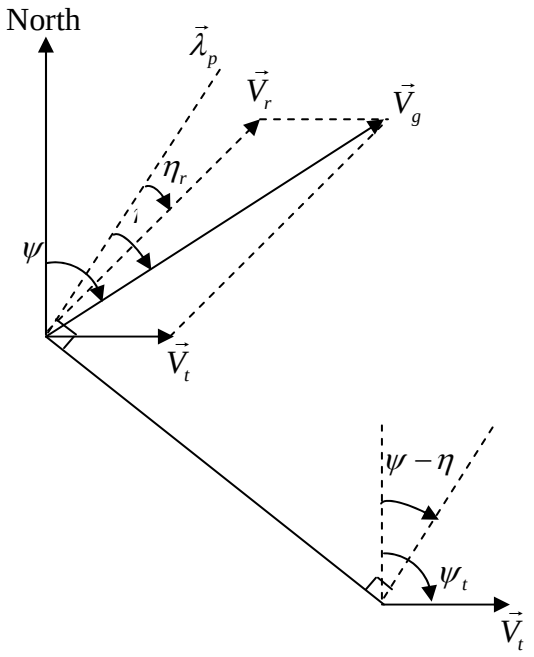

Figure 6. Decomposition of SUAV velocity vector $\vec{V}_g$

Consider the decomposition of the SUAV ground vector $\vec{V}_g$ as shown in Figure 6 [4],

$$\vec{V}_g = \vec{V}_t + \vec{V}_r \tag{23}$$

where $\vec{V}_t$ is the target velocity vector, and $\vec{V}_r = \vec{V}_g - \vec{V}_t$ is the remaining velocity vector. The following relationships are then derived:

$$V_g \cos\eta = V_r \cos\eta_r + V_t \cos\left[\psi_t - (\psi - \eta)\right] \tag{24a}$$

$$V_g \sin\eta = V_r \sin\eta_r + V_t \sin\left[\psi_t - (\psi - \eta)\right] \tag{24b}$$

where η_r is the angle between $\vec{V}_r$ and $\vec{\lambda}_p$.

Substituting Equations (24a) and (24b) into Equations (19a) and (19b), the system kinematics can be written as:

$$\dot{\eta} = -\frac{V_r}{\rho}\cos\eta_r + \dot{\psi} \tag{25a}$$

$$\dot{\rho}_e = -V_r \sin\eta_r \tag{25b}$$

Since $\eta_r = 0$ leads to $\dot{\rho}_e = 0$, this suggests that $\eta_r = 0$ can be the control objective.

Assuming that the target velocity V_t is constant with constant heading, this composition can be interpreted by considering the target coordinate frame (T-frame), whose origin is fixed on the target. In this frame, the target is static and the SUAV is flying with time-varying velocity $V_r(t)$ with the angle $\dot{\eta}_r(t)$ from $\vec{\lambda}_p$. The dynamics for $\eta_r(t)$ can be written as:

$$\dot{\eta}_r(t) = -\frac{V_r(t)}{\rho(t)}\cos\eta_r(t) + u_r(t) \tag{26}$$

where $u_r(t)$ is the turn rate of the "virtual SUAV" with velocity $V_r(t)$.

To find the relationship between $u_r(t)$ and $\dot{\psi}(t)$, assume that the target is moving with constant velocity and heading, and take derivative of Equation (26). Then, from classical mechanics:

$$\dot{V}_r\vec{n}_r + \vec{u}_r \times \vec{V}_r = \vec{u}_g \times \vec{V}_g \tag{27}$$

where $\vec{u}_g$ denotes the three dimensional angular velocity vector for the SUAV, $\vec{n}_r$ is the normalized vector in the direction of $\vec{V}_r$. Since $\vec{u}_r \times \vec{V}_r$ is perpendicular to $\vec{n}_r$, taking the inner product of both sides of Equation (27) with $\vec{n}_r$ gives:

$$\dot{V}_r = \left(\vec{u}_g \times \vec{V}_g\right).\vec{n}_r \tag{28}$$

Substituting Equation (28) into Equation (27) gives:

$$\left(\left(\vec{u}_g \times \vec{V}_g\right).\vec{n}_r\right)\vec{n}_r + \vec{u}_r \times \vec{V}_r = \vec{u}_g \times \vec{V}_g \tag{29}$$

Since the two terms on the left hand side of Equation (29) are perpendicular to each other, this implies that:

$$\left|\left(\vec{u}_g \times \vec{V}_g\right).\vec{n}_r\right|^2 + \left|\vec{u}_r \times \vec{V}_r\right|^2 = \left|\vec{u}_g \times \vec{V}_g\right|^2$$

$$u_r = \frac{\sqrt{{V_g}^2 {V_r}^2 - \left|\vec{V}_g \times \vec{V}_t\right|^2}}{{V_r}^2} u_g \tag{30}$$

Thus, the kinematics of the system in the T-frame is given by:

$$\dot{\eta}_r = -\frac{V_r(t)}{\rho(t)}\cos\eta_r(t) + m(t)\dot{\psi}(t) \tag{31a}$$

$$\dot{\rho}_e = -V_r(t)\sin\eta_r(t) \tag{31b}$$

where $m(t) = \dfrac{\sqrt{{V_g}^2 {V_r}^2(t) - \left|\vec{V}_g \times \vec{V}_t(t)\right|^2}}{{V_r}^2(t)}$, $\qquad V_r = \left|\vec{V}_g - \vec{V}_t\right|$

The new control objective is to regulate $\eta_r(t)$ to 0 and thus drive $\rho(t)$ to ρ_d (which is the desired range to target). To achieve this, the control law for implementation on the SUAV autopilot controller is as shown below:

$$\dot{\psi} = \frac{1}{m(t)}\left(-k_1\eta_r(t) + \frac{V_r(t)}{\rho(t)}\cos\eta_r(t)\right) \tag{32}$$

Thus, the feedback system consisting of Equations (19) and Equation (32) is given by:

$$\dot{\eta}(t) = -k_1\eta_r(t) + V_r(t)\left(\frac{1}{\rho_d} - \frac{1}{\rho(t)}\right)\cos\eta_r(t) \tag{33a}$$

$$\dot{\rho}_e(t) = -V_r(t)\sin\eta_r(t) \tag{33b}$$

F. SUMMARY OF THE CONTROL LAW DESIGNS

Based on the information gathered from previous works, a summary of the pros and cons of each control law design is presented in Table 1.

	Current Control Law	New Control Law
Pros	- Simple to implement. - Relies exclusively on passive information gathered from the image processing software.	- Perfect range holding capability.
Cons	- Range holding capability depends on the target motion.	- Requires information on target velocity and heading.

Table 1. Comparison of Control Law Designs

G. TRACKING LOSS EVENTS

Due to space and computational power constraint, the image based tracking software cannot be placed onboard the SUAV and the visual part of the control loop has to be closed on the ground. Hence, a critical issue that must be addressed by the VBTT algorithm is its performance in the presence of tracking loss events defined here as any event that causes the image processing software to lose tracking of the target. From the experience gathered from previous flight tests, this event occurs primarily due to the dynamic change of lighting conditions and radio frequency interference in video and control links. The tracking loss can be defined as a binary signal [2]:

$$s(t) = \begin{cases} 0 & \text{out-of frame event at time t,} \\ 1 & \text{camera tracks target at time t.} \end{cases} \tag{34}$$

For a given binary signal $s(t)$, let $T_s(\tau, t)$ denote the length of time in the interval $[\tau, t]$ when $s(t) = 0$. Then, formally,

$$T_s(\tau, t) = \int_{\tau}^{t} \left(1 - s(\omega)\right) d\omega \tag{35}$$

The image processing software will experience a brief target loss event if:

$$T_s(\tau,t) \le T_0 + \alpha(t-\tau), \qquad t \ge \tau \ge 0, \tag{36}$$

for some $T_0 \ge 0$ and $\alpha \in [0,1]$. The scalar T_0 is called the instability bound and α is called the asymptotic instability ratio. α will provide am asymptotic upper bound on the ratio $T_s(\tau,t)/(t-\tau)$, as $(t-\tau) \to \infty$.

From previous work [2], [5], both control laws are expected to suffer predictable degradation in performance when tracking loss events (TLE) occur.

THIS PAGE INTENTIONALLY LEFT BLANK

III. IMPLEMENTATION OF CONTROL LAW

A. FAST ESTIMATION OF TARGET MOTION

As seen from Equation (32), the new control law requires information on the target velocity and heading in order for it to generate the appropriate control input $\dot{\psi}$ for the autopilot. A fast estimator can be applied to generate an estimation of the target velocity and heading [11]. The target motion estimation consists of two steps. Firstly, the target position is calculated based on the available measurements. Thereafter, the target velocity and heading is estimated using the fast estimator.

1. Calculation of Target Position

The relative position between the target and the SUAV in the I-frame and C-frame are denoted by $p = \left[p_x, p_y, p_z \right]^T$ and $p_c = \left[x_c, y_c, z_c \right]^T$ respectively. Thus, the following relationship can be derived:

$$\begin{bmatrix} x_c \\ y_c \\ z_c \end{bmatrix} = {}^{C}_{B}R\,{}^{B}_{I}R \begin{bmatrix} p_x \\ p_y \\ p_z \end{bmatrix} = {}^{C}_{B}R\,{}^{B}_{I}R \begin{bmatrix} p_x \\ p_y \\ h \end{bmatrix} \tag{37}$$

where ${}^{C}_{B}R$ and ${}^{B}_{I}R$ can be obtained using the Euler angles of the SUAV and the pan/tilt angles of the camera provided the onboard IMU. Assuming the camera follows the pin-hole model,

$$\begin{bmatrix} y_c/x_c \\ z_c/x_c \end{bmatrix} = \begin{bmatrix} u/F \\ v/F \end{bmatrix} \tag{38}$$

where F is the focal length of the camera and (u, v) is the position of the target image in the P-frame. Thus, Equation (37) can be rewritten as:

$$\begin{bmatrix} 1 \\ y_c/x_c \\ z_c/x_c \end{bmatrix} = \begin{bmatrix} 1 \\ u/F \\ v/F \end{bmatrix} = {}^{C}_{B}R\,{}^{B}_{I}R \begin{bmatrix} p_x/x_c \\ p_c/x_c \\ h/x_c \end{bmatrix} \tag{39a}$$

$$\begin{bmatrix} p_x/x_c \\ p_c/x_c \\ h/x_c \end{bmatrix} = \left({}^{C}_{B}R\,{}^{B}_{I}R \right)^{-1} \begin{bmatrix} 1 \\ u/F \\ v/F \end{bmatrix} \tag{39b}$$

Hence, $\left(p_x, p_y \right)$ can be calculated since all the terms of the right hand side of Equation (39) are known. The target in the I-frame can be obtained using the SUAV position in the I-frame given by the onboard GPS.

$$p_{target} = p_{uav} + p = p_{uav} + \begin{bmatrix} p_x \\ p_y \\ h \end{bmatrix} \tag{40}$$

2. Estimation of Target Velocity and Heading

Let $x(t) = \left[p_x(t), p_y(t) \right]^T$ be the horizontal component of $p(t)$ that has being calculated in the previous section. From Figure 4, $x(t)$ satisfies the following kinematics:

$$\dot{x}(t) = \begin{bmatrix} \dot{p}_x(t) \\ \dot{p}_y(t) \end{bmatrix} = -V_g(t) \begin{bmatrix} \sin\psi(t) \\ \cos\psi(t) \end{bmatrix} + V_t(t) \begin{bmatrix} \sin\psi_t(t) \\ \cos\psi_t(t) \end{bmatrix} \tag{41}$$

Define the second term of Equation (41) as:

$$\omega(t) = V_t(t) \begin{bmatrix} \sin\psi_t(t) \\ \cos\psi_t(t) \end{bmatrix}, \qquad \omega(0) = \omega_0$$

The estimate of the target velocity $\hat{V}_t(t)$ and heading $\dot{\psi}_t(t)$ can be obtained through the following steps:

a. State Predictor

$$\dot{\hat{x}}(t) = A_m \tilde{x}(t) - V_g(t) \begin{bmatrix} \sin\psi(t) \\ \cos\psi(t) \end{bmatrix} + \hat{\omega}(t), \qquad \hat{x}(0) = x_0 \tag{42}$$

where $\tilde{x}(t) = \hat{x}(t) - x(t)$ and A_m is a known Hurwitz matrix chosen to satisfy the performance requirements.

b. Adaptive Law

$$\dot{\hat{\omega}}(t) = \Gamma_c \,\mathrm{Pr}oj\left(\hat{\omega}(t), -P\tilde{x}(t)\right), \qquad \hat{\omega}(0) = \hat{\omega}_0 \tag{43}$$

where $\Gamma_c > 0$ determines the adaptation rate, chosen sufficiently large to ensure fast convergence, P is the solution of the algebraic Lyapunov equation $A_m{}^T P + PA_m = -Q$ for some choice of matrix $-Q < 0$ and $\mathrm{Pr}oj(\bullet,\bullet)$ is the projective operator which keeps the parameter within the pre-defined bound.

c. Low-Pass Filter

$$\omega_r(s) = C(s)\omega(s), \quad \omega_r(0) = \hat{\omega}_0 \tag{44a}$$

$$\omega_e(s) = C(s)\omega(s), \quad \omega_e(0) = \hat{\omega}_0 \tag{44b}$$

where $C(s)$ is a diagonal matrix with its i$^{\text{th}}$ diagonal element $C_i(s)$ being a strictly proper stable transfer function with low-pass gain $C_i(0) = 1$ for $i = 1, 2$.

d. Extraction of $\hat{V}_t(t)$ and $\hat{\psi}_t(t)$ from $\omega_e(t)$

The target velocity and heading can then obtained from the following relationships:

$$\hat{V}_t(t) = \sqrt{\omega_{e1}^2(t) + \omega_{e2}^2(t)} \tag{45a}$$

$$\hat{\psi}_t(t) = \tan^{-1}\left(\frac{\omega_{e1}(t)}{\omega_{e2}(t)}\right) \tag{45b}$$

More of theoretical details on the development of performance bounds can be found in [5] and [11].

B. CONTROL SYSTEM ARCHITECTURE

The control architecture that implements the control law is presented in Figure 7 [2]. It consists of an autopilot and a gimbal driven by the control inputs $\dot{\psi}$ and $\dot{\psi}_h$. The onboard CCD camera provides real-time imagery to the image tracking software. When target lock is engaged, the image tracking software will compute the camera LOS pan error ε. The onboard GPS and INS will in turn provide the solution for the navigation error η.

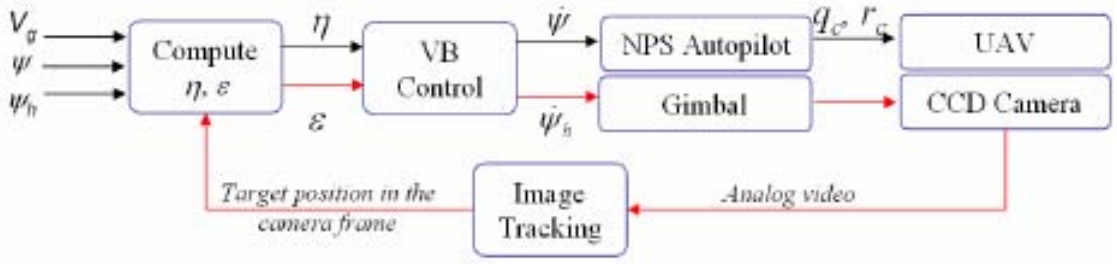

Figure 7. Control System Architecture

C. SIMULINK MODEL SCHEMATIC

The VBTT SIMULINK model schematic for the current control law in Equation (21a) is presented in Figure 8.

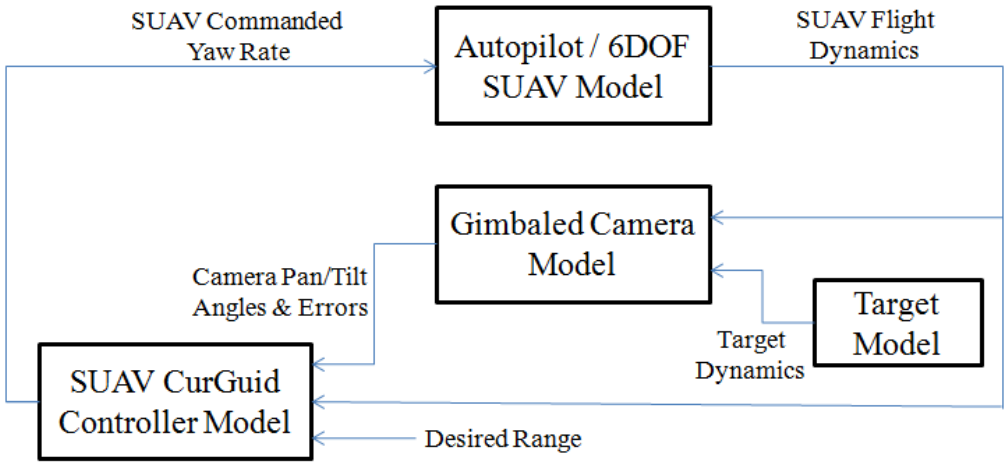

Figure 8. VBTT SIMULINK Model Schematic for Current Control Law

The current control law for the SUAV yaw rate command $\dot{\psi}$ is being implemented in the "CurGuid Controller" block (see Figure 9).

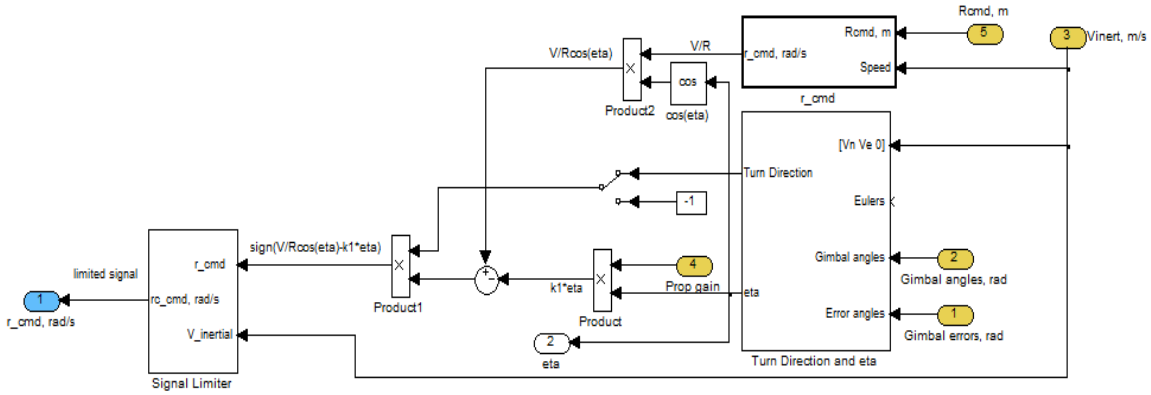

Figure 9. "CurGuid Controller Block" for Implementation of Current Control Law

The VBTT SIMULINK model schematic for the new control law in Equation (32) is presented in Figure 10. Comparing Figure 8 and 10, the main difference between the two schematics is that the VBTT SIMULINK model schematic for the current control law does not include the "Target Estimator" block, since the current control law relies exclusively on the information gathered from the image processing software.

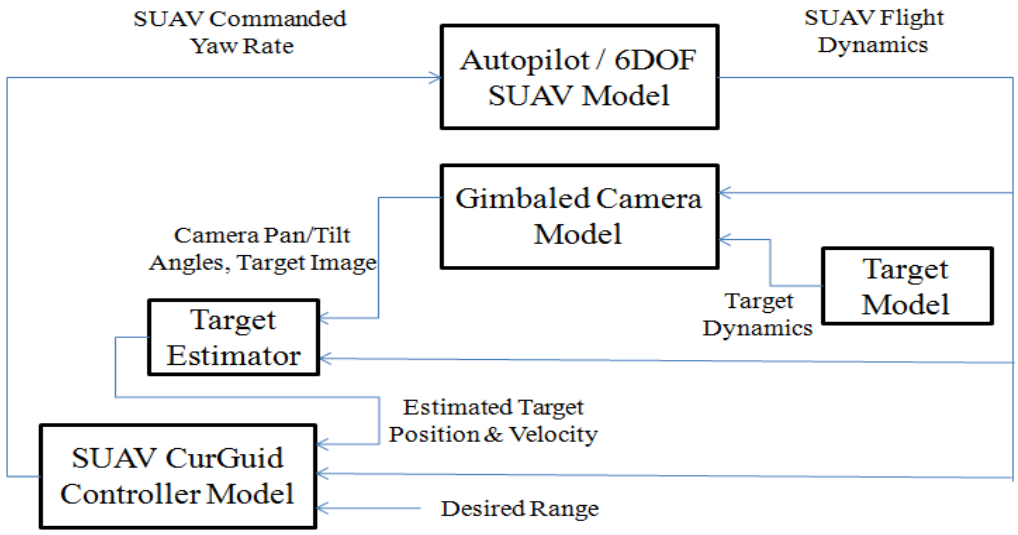

Figure 10. VBTT SIMULINK Model Schematic for New Control Law

The new control law for the SUAV yaw rate command $\dot{\psi}$ is being implemented in the "CurGuid Controller" block (see Figure 11).

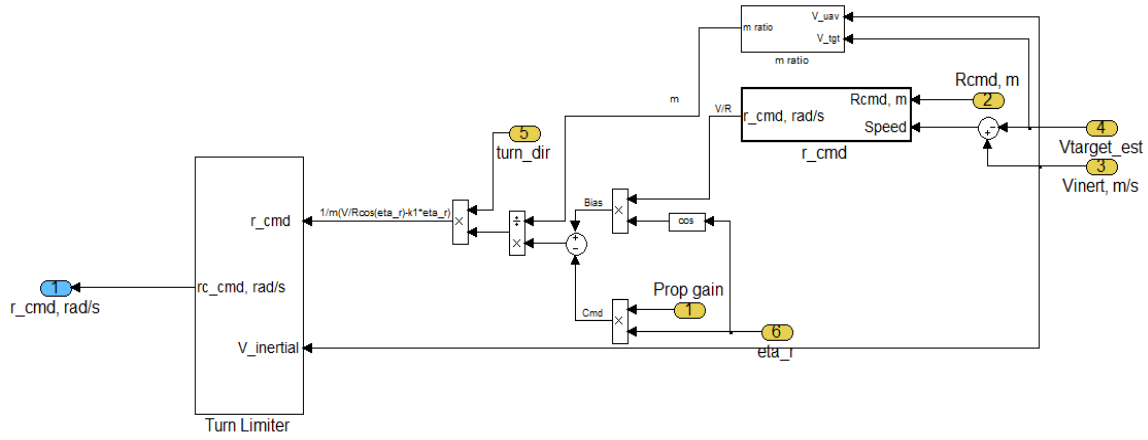

Figure 11. "CurGuid Controller Block" for Implementation of New Control Law

D. L_1 ADAPTIVE CONTROLLER FOR GIMBALED CAMERA LOOP

To guarantee the transient performance of the gimbaled pan turning and its robustness to time-delay due to image processing and varying communication conditions, a newly developed L_1 adaptive controller is applied to the gimbaled pan control loop [12], [11]. For simplicity of notation, let $u_h(t) = -\dot{\psi}_h(t)$. Therefore, Equation (19) can be rewritten as:

$$\dot{\varepsilon}(t) = a_m \varepsilon(t) + u_h(t) + \alpha\varepsilon(t) + \sigma(t) \tag{46}$$

where $a_m < 0$, $\alpha = -a_m$, $u_h(t) = -\dot{\psi}_h(t)$,

$$\sigma(t) = \frac{V_g \cos\eta(t) - V_t \cos\left[\psi_t(t) - \left(\psi(t) - \eta(t)\right)\right]}{\rho(t)} - \dot{\psi}(t)$$

The L_1 adaptive controller consists of the state predictor, the adaptive law and the control law given in the following steps:

1. State Predictor

$$\dot{\hat{\varepsilon}}(t) = a_m \hat{\varepsilon}(t) + u_h(t) + \hat{\alpha}(t)\varepsilon(t) + \hat{\sigma}(t), \qquad \hat{\varepsilon}(0) = \varepsilon_0 \tag{47}$$

2. Adaptive Law

The parameter estimations $\hat{\alpha}(t)$ and $\hat{\sigma}(t)$ are governed by the following adaptive laws:

$$\dot{\hat{\alpha}}(t) = \Gamma \Pr oj\left(\hat{\alpha}(t), -\tilde{\varepsilon}(t)\varepsilon(t)\right), \qquad \hat{\alpha}(0) = \hat{\alpha}_0 \tag{48a}$$

$$\dot{\hat{\sigma}}(t) = \Gamma \Pr oj\left(\hat{\sigma}(t), -\tilde{\varepsilon}(t)\right), \quad \hat{\sigma}(0) = \hat{\sigma}_0 \tag{48b}$$

where $\Gamma_c > 0$ determines the adaptation rate and $\tilde{\varepsilon}(t) = \hat{\varepsilon}(t) - \varepsilon(t)$. The projection operators ensure that the parameters are kept within the predefined bounds.

3. Control Law

The control signal $u_h(t)$ is generated through the feedback of the following systems:

$$\chi(s) = D(s)\bar{r}(s) \tag{49a}$$

$$u_h(s) = -k\chi(s) \tag{49b}$$

where $k > 0$ and $D(s)$ is any transfer function which leads to a strictly proper stable transfer function:

$$\bar{C}(s) = \frac{kD(s)}{1 + kD(s)} \tag{50}$$

More of theoretical details on the development of performance bounds can be found in [5] and [12].

THIS PAGE INTENTIONALLY LEFT BLANK

III. SIMULATION RESULTS

A. SELECTION OF MEASURE OF PERFORMANCE

The performance of the new control law is examined for variation in feedback control parameter k_1, the relative velocity ratio of the target and SUAV V_t/V_g and the "frequency" of tracking loss events. The results obtained are then compared to those that were obtained in previous work for the current control law [9] – [10].

To evaluate the performance of the new control law, three measures of performance (MOP), M_1, M_2 and M_3 are being devised. These three MOP are assumed to be independent of each other. The physical meaning and definition of each MOP are as follows:

The first MOP, M_1 is defined as inverse of the ratio of the captured range over the convergence time. The convergence time is the time taken for the SUAV to converge to its first zero crossing of ρ_0, while the captured range is the radial range that is covered by the SUAV during the convergence period. A lower value for M_1 is desired, as it represents a faster range capturing capability.

The second MOP, M_2 is devised to measure the time-averaged deviation from the commanded range. The deviation from the commanded range is only measured after the SUAV's first closest approach. A lower value for M_2 is desired, as it represents better range holding capability of the SUAV.

The final MOP, M_3 is devised to measure the time-averaged navigation error. The navigation error η_r is the angle between the virtual UAV's ground velocity vector ($\vec{V}_r$) and the normal to LOS vector ($\vec{\lambda}_p$) and it is only measured after the SUAV's first closest approach. As seen from Equation (33b), regulating η_r to zero will in turn drive the range to target to the desired range. Hence, a lower value for M_3 is desired, as it indicates better range holding capability of the SUAV.

B. SENSITIVITY ANALYSIS OF MOP TO VARIATIONS IN k_1

The sensitivity analysis of the new control law to variations of feedback control parameter k_1 is examined in a scenario where the target is moving with a constant heading and the commanded range is 300m. This scenario is chosen as a baseline model for further comparison with other target motion scenarios. The initial conditions are: (1) SUAV velocity = 25 m/s; (2) Target velocity = 8 m/s; (3) Initial position of the SUAV is at [-1000, 0, 500] and (4) Initial position of the target is at [0, 0, 0]. Thus, the initial horizontal ground range from the SUV to target is 700m.

Performance of M_1, M_2, M_3 and M_0 with Variations to k_1

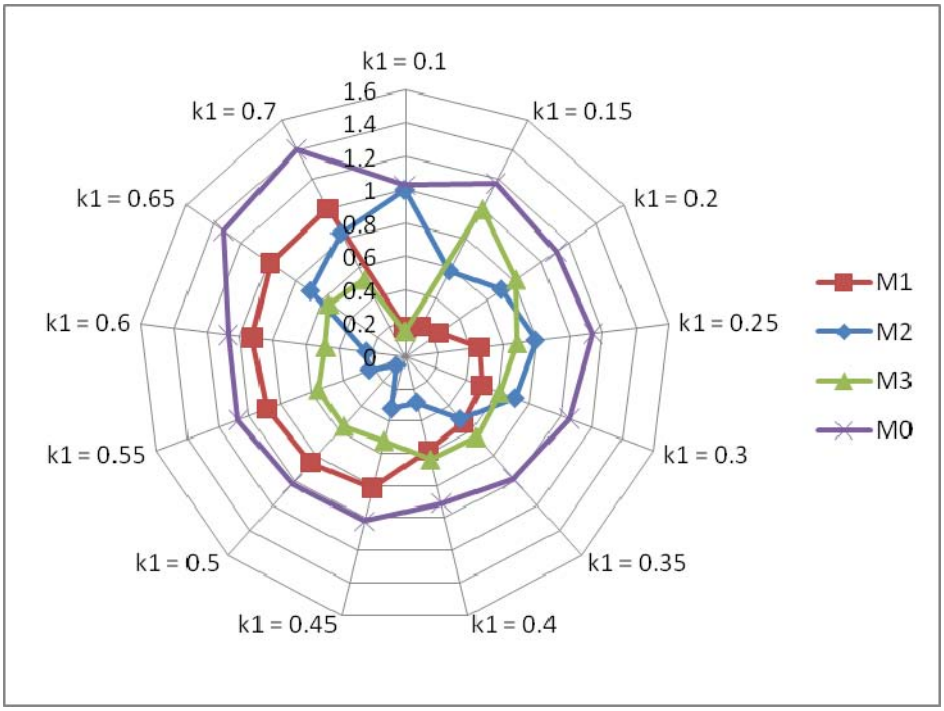

Figure 12. Variation of M_1, M_2, M_3 and M_0 versus k_1

The following observations can be made from the plot as shown in Figure 12:

(a) It is observed that M_1 increases with increasing k_1. This in turn means that the convergence speed is decreasing with increasing k_1. A higher value of k_1 causes the SUAV to incur a higher overshoot. As a result, the SUAV will take a longer time to converge to the desired range to target. It is also observed M_3 decreases with increasing k_1. M_2 also decreases with increasing k_1 till k_1 reaches a value of 0.5. Thereafter, M_2 starts to increase with increasing k_1.

(b) As M_1, M_2 and M_3 varies differently with increasing k_1, there is an obvious need to introduced a new MOP for the purpose of finding an optimal trade off among the criteria [10]. Therefore, M_0 is introduced as the square root of the sum of squares of the three independent parameters:

$$M_0 = \sqrt{M_1^2 + M_2^2 + M_3^2} \tag{48}$$

The parameters are properly scaled before the convolution; the discussion is not a subject of this thesis work. The choice of the MOP is motivated by the fact that k_1 can be represented by a point in a three dimensional (3-D) space defined by the three MOP {M_1, M_2, M_3}. As the control objective is the minimize all three MOP, this corresponds to a search for a value of k_1 such that the distance from the origin of this 3-D space is minimized as graphically shown in Figure 13.

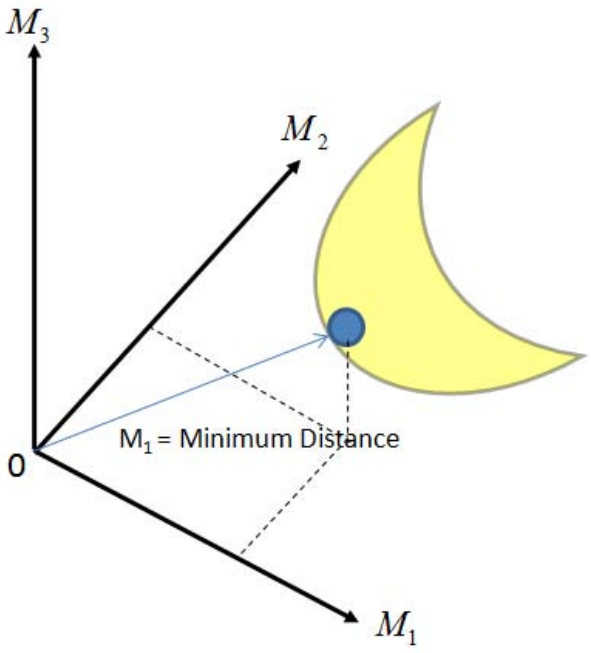

Figure 13. Motivation for Multi-Criteria Optimization

(c) From Figure 12, it is also observed that M_0 attains a minimum value when k_1 is at a value of 0.4. Thus, k_1 is set to 0.4 for the remaining experiments as it provides us with the optimal performance for the new control law.

Figure 14 presents the results obtained for the new control law when k_1 is set to 0.4.

14(a) SUAV & Target Trajectory

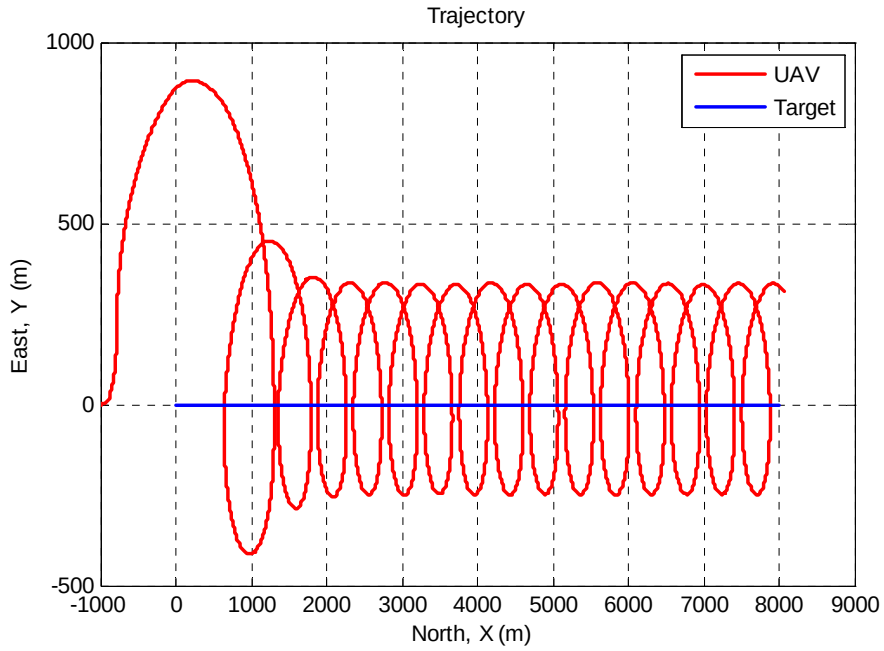

14(b) Range Convergence, Range Holding & Navigation Angle Error Performance

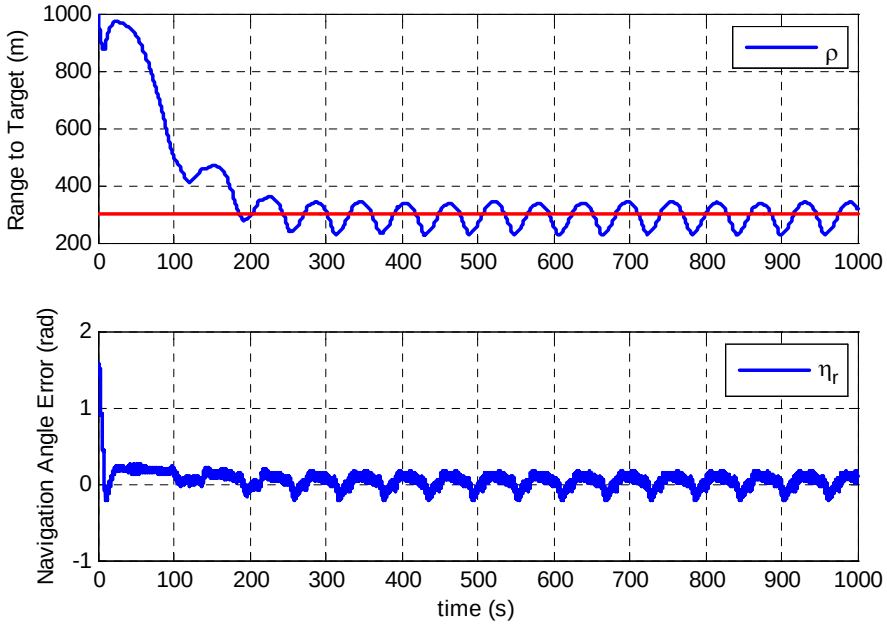

14(c) SUAV Pan & Tilt Errors

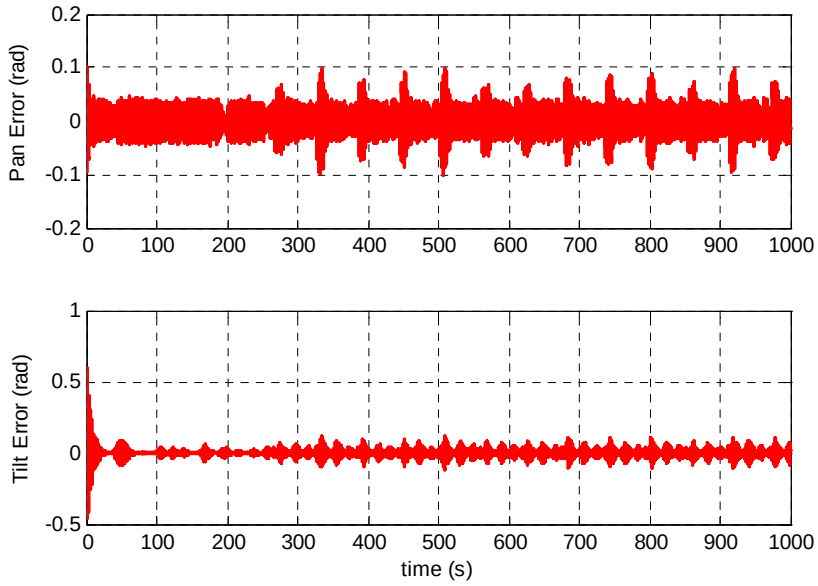

14(d) Target Estimator Performance

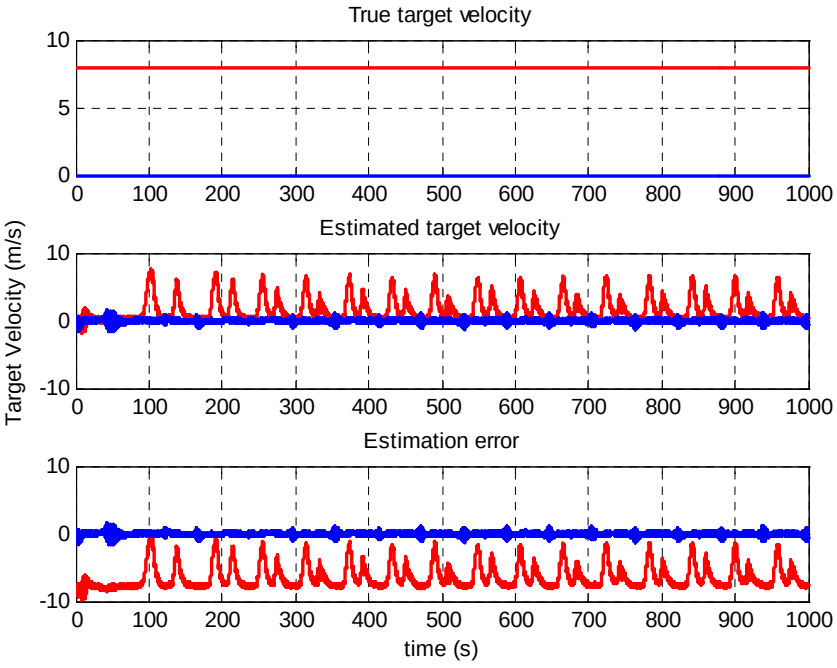

Figure 14. Sensitivity Analysis for $k_1 = 0.4$ (Optimal Case)

C. SENSITIVITY ANALYSIS OF MOP TO VARIATIONS IN V_t/V_g

The sensitivity analysis of the new control law to variations in V_t/V_g is examined in a scenario where the target is moving with a constant heading and the commanded range is 300m. The initial conditions are: (1) SUAV velocity = 25 m/s; (2) Initial position of the SUAV is at [-1000, 0, 500]; (3) Initial position of the target is at [0, 0, 0] and (4) $k_1 = 0.4$. Thus, the initial horizontal ground range from the SUV to target is 700m.

M_0, which is defined in the previous experiment, will be utilized to access the sensitivity performance of the new control law to variations in V_t/V_g.

Performance of M_1, M_2, M_3 and M_0 with Variations to V_t/V_g

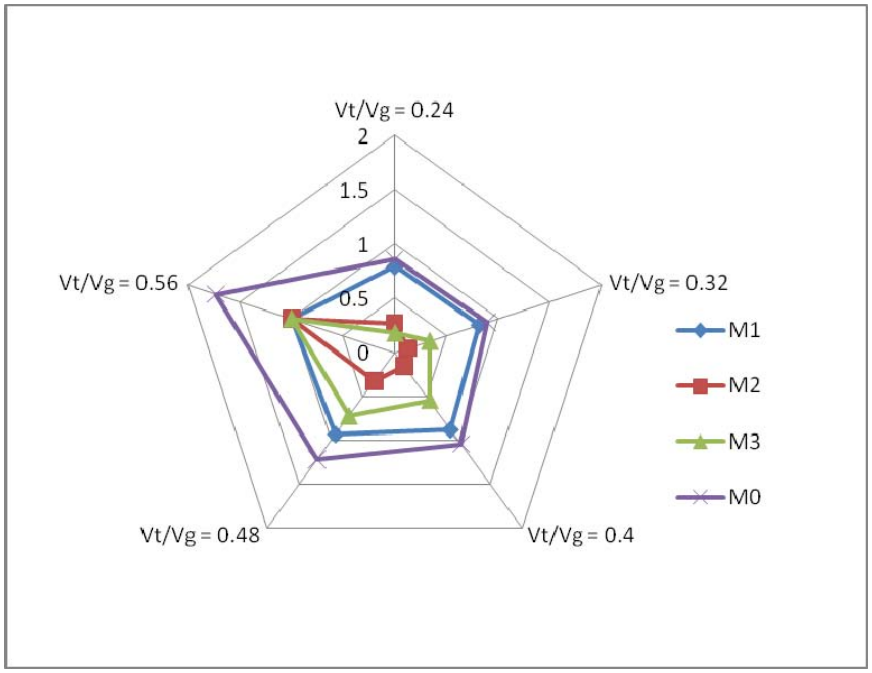

Figure 15. Variation of M_1, M_2, M_3 and M_0 versus Speed Ratio V_t/V_g

The following observations can be made from the plot as shown in Figure 15:

(a) It is observed that M_1 increases with increasing V_t/V_g. This in turn means that the convergence speed is decreasing with increasing V_t/V_g. As the target velocity

increases, the SUAV takes a longer time to converge to the desired range to target. It is also observed that both M_2 and M_3 increases with increasing V_t/V_g. In particular, M_2 increases substantially when V_t/V_g is at a value of 0.56.

(b) From Figure 15, it is also observed that M_0 increases with increasing V_t/V_g. Similar to M_2, M_0 increases substantially when V_t/V_g is at a value of 0.56. This suggests that the performance of the new control law degrades drastically when the target velocity is more than half of the SUAV velocity.

Figure 16 to 20 presents the detailed results obtained for the new control law when V_t/V_g is varied from $6/25$ to $14/25$.

Case 1: $V_t/V_g = 6/25$

16(a) SUAV & Target Trajectory

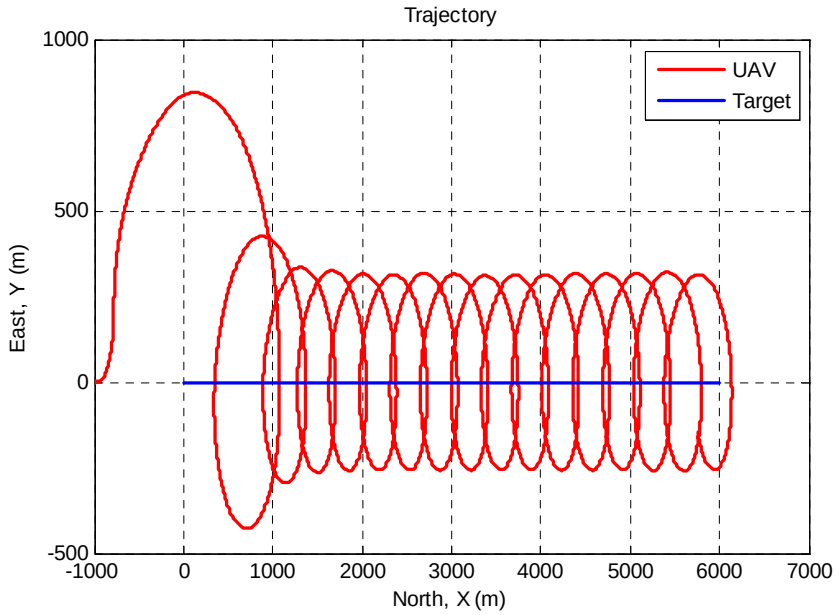

16(b) Range Convergence, Range Holding & Navigation Angle Error Performance

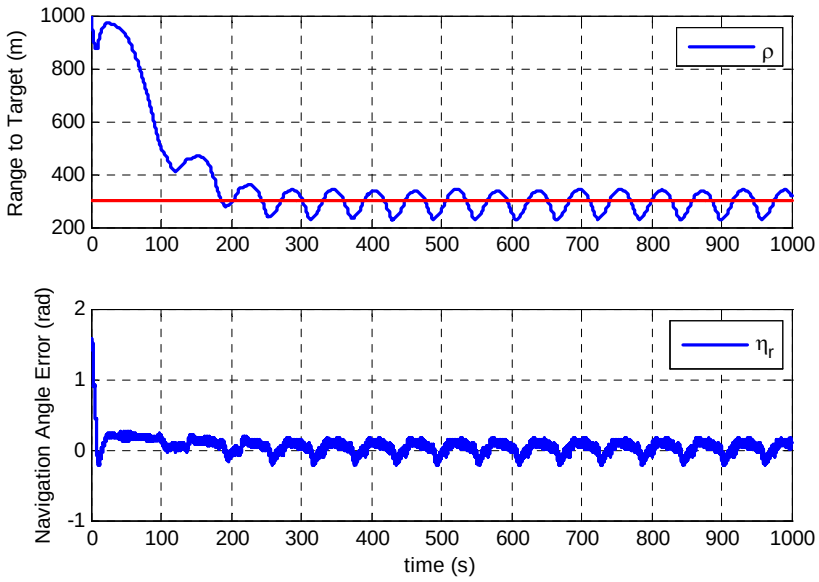

16(c) SUAV Pan & Tilt Errors

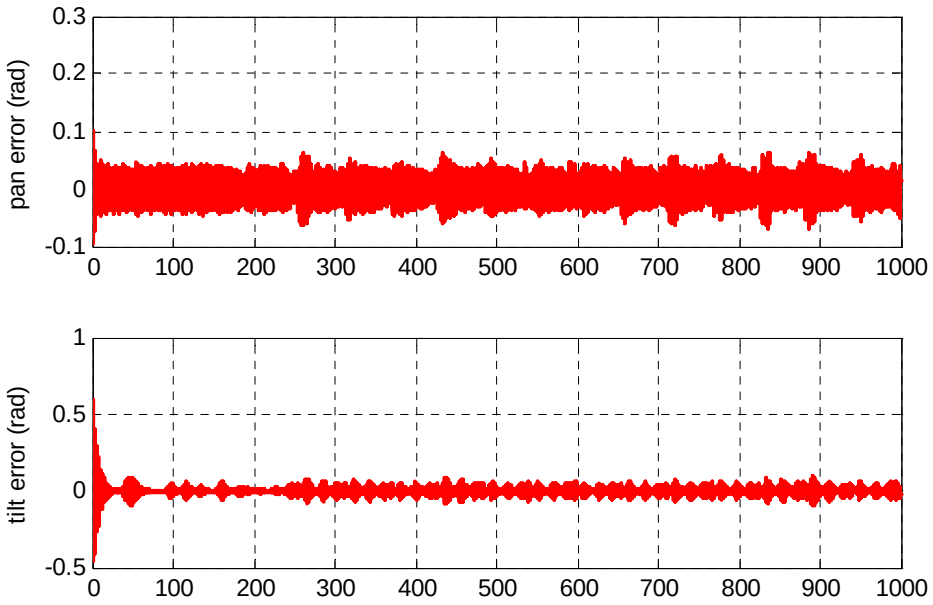

16(d) Target Estimator Performance

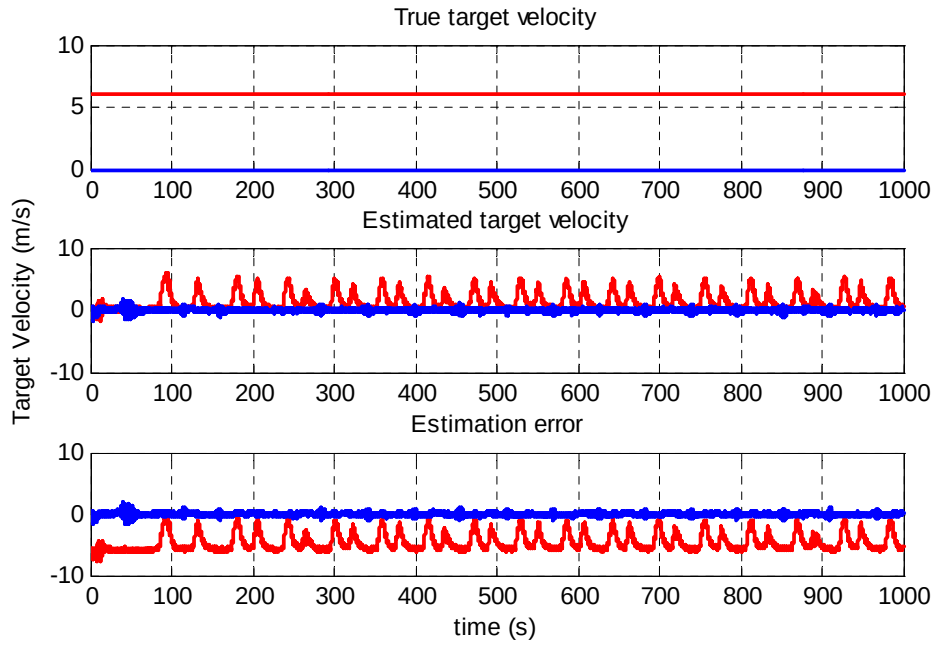

Figure 16. Sensitivity Analysis for $V_t/V_g = 6/25$

Case 2: $V_t/V_g = 8/25$

17(a) SUAV & Target Trajectory

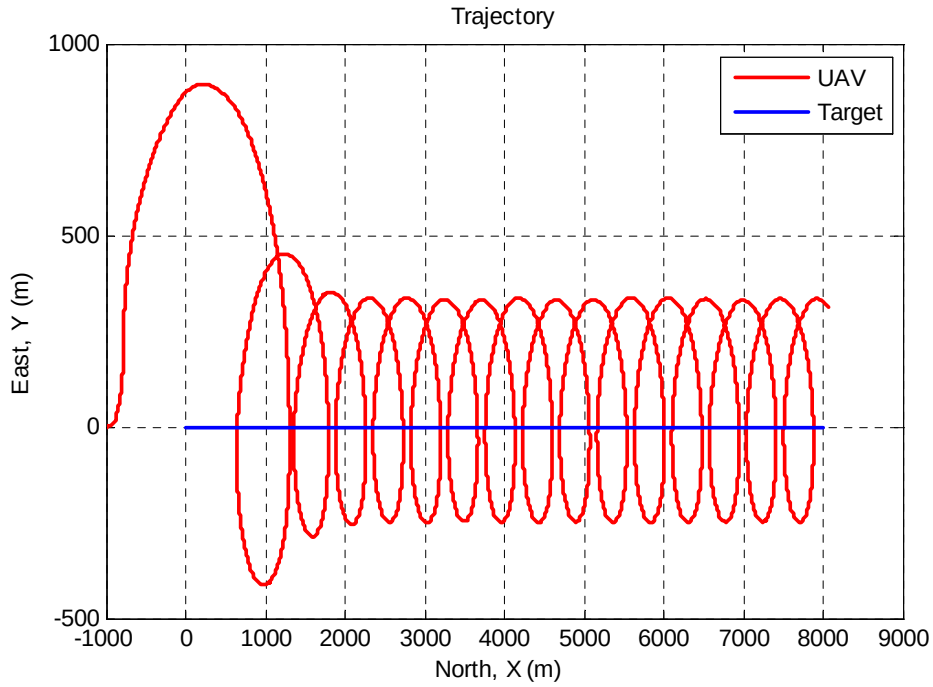

17(b) Range Convergence, Range Holding & Navigation Angle Error Performance

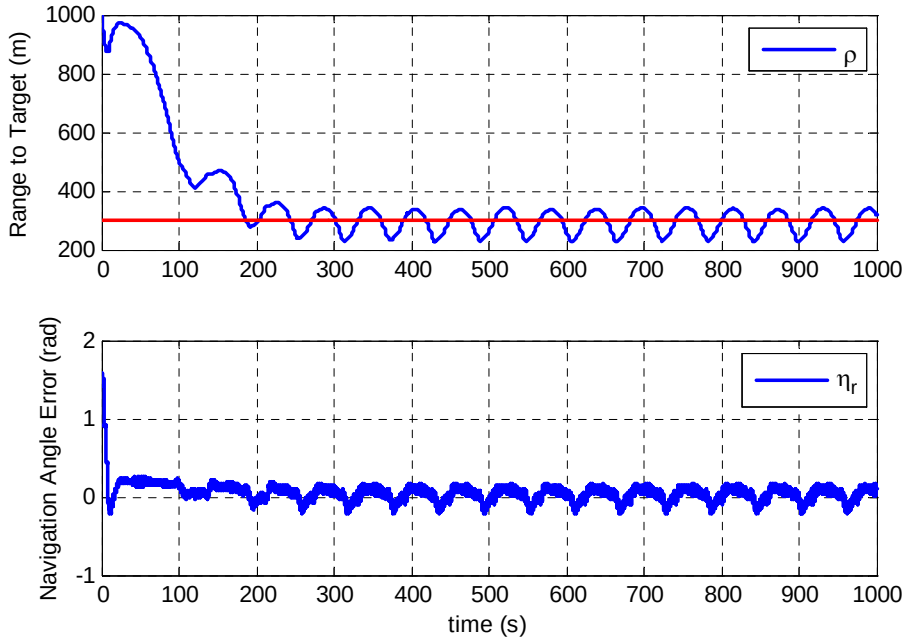

17(c) SUAV Pan & Tilt Errors

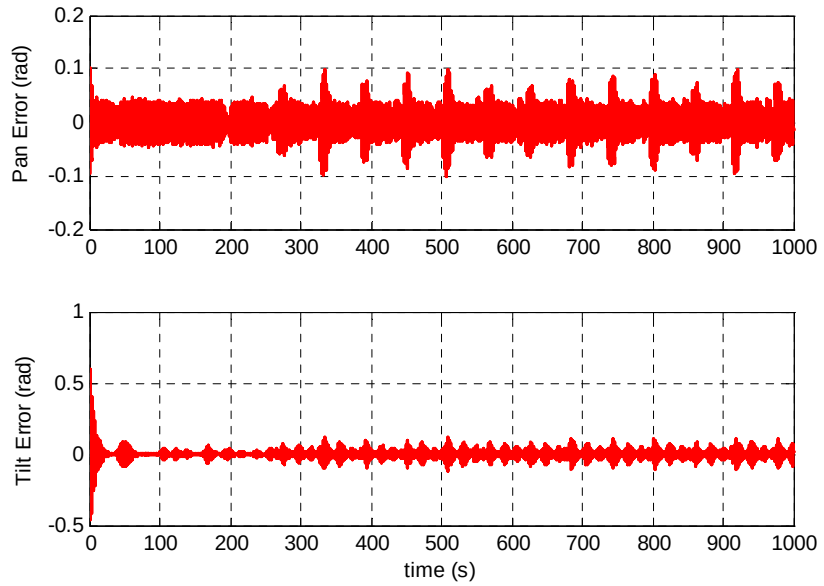

17(d) Target Estimator Performance

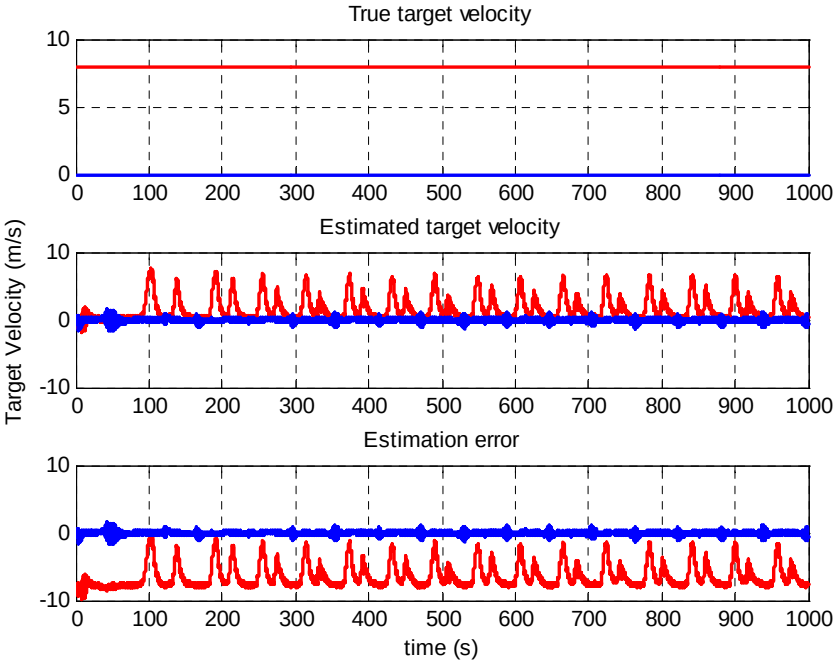

Figure 17. Sensitivity Analysis for $V_t/V_g = 8/25$

Case 3: $V_t/V_g = 10/25$

18(a) SUAV & Target Trajectory

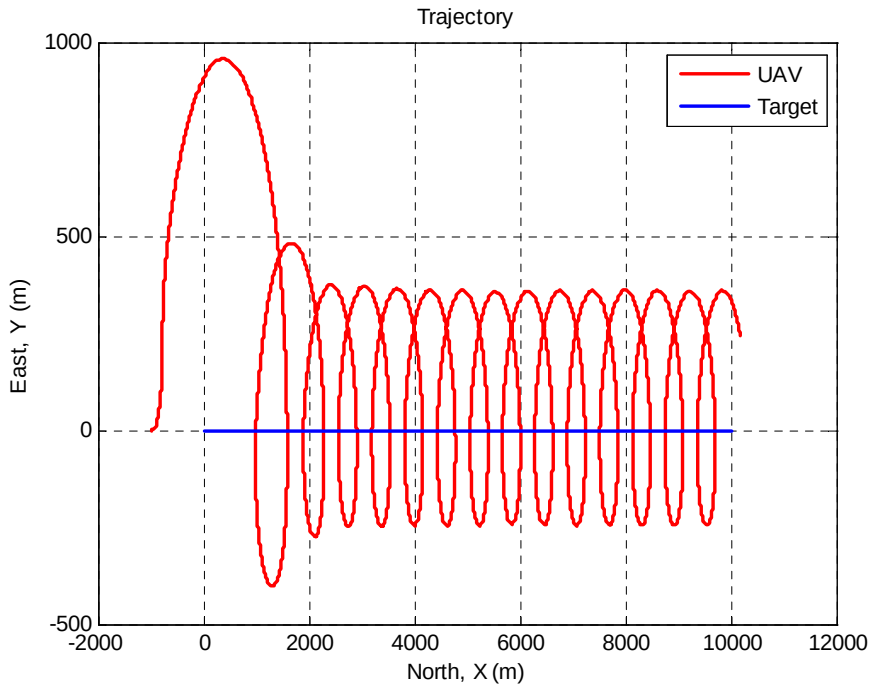

18(b) Range Convergence, Range Holding & Navigation Angle Error Performance

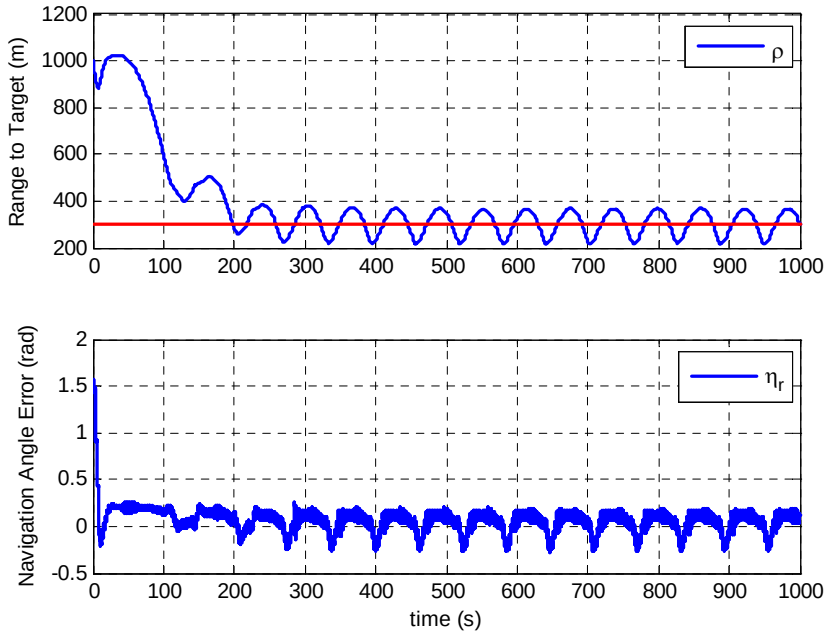

18(c) SUAV Pan & Tilt Errors

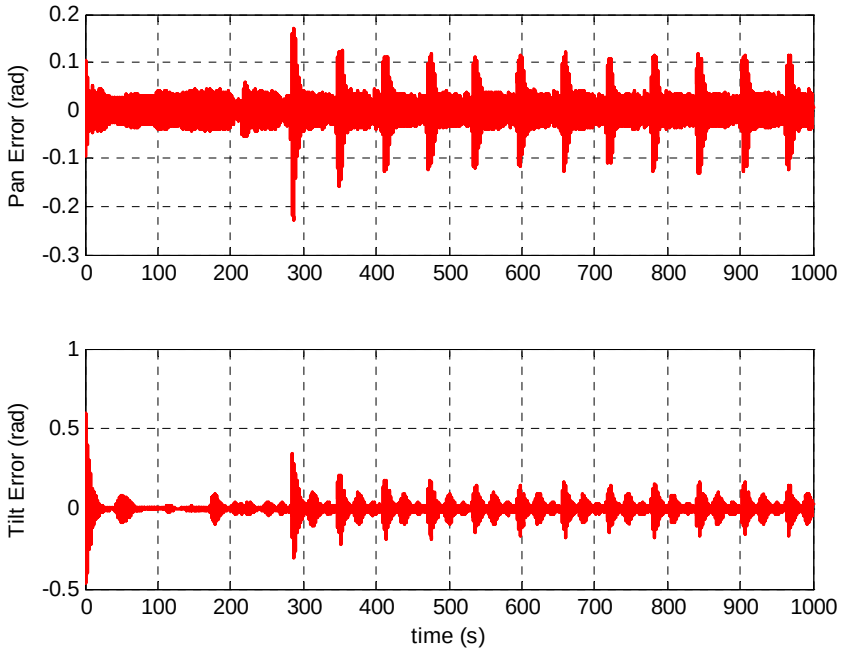

18(d) Target Estimator Performance

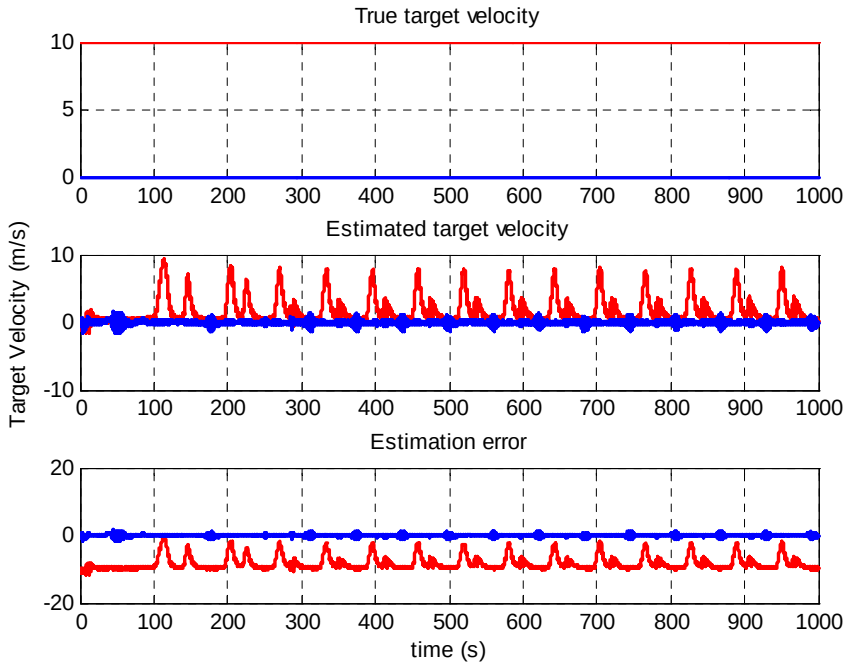

Figure 18. Sensitivity Analysis for $V_t/V_g = 10/25$

Case 4: $V_t/V_g = 12/25$

19(a) SUAV & Target Trajectory

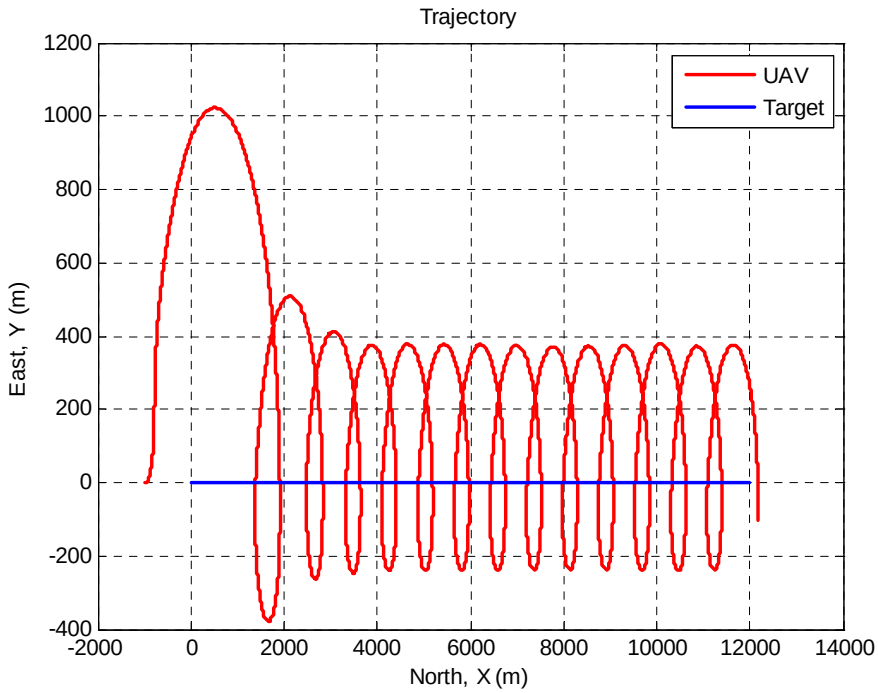

19(b) Range Convergence, Range Holding & Navigation Angle Error Performance

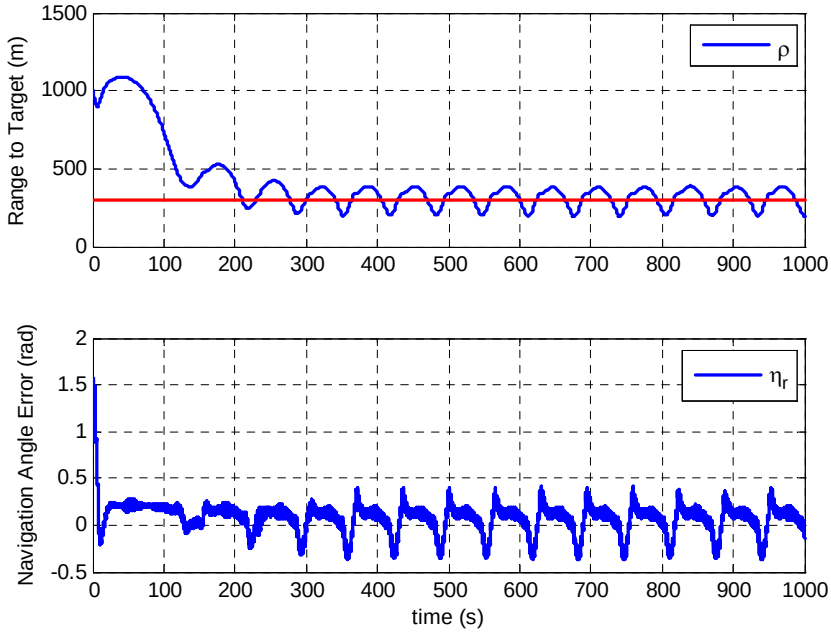

19(c) SUAV Pan & Tilt Errors

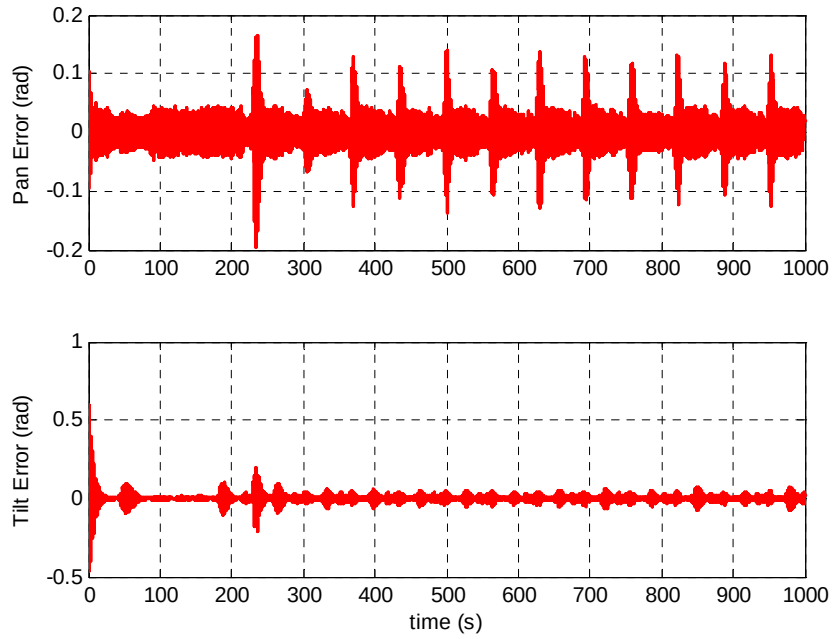

19(d) Target Estimator Performance

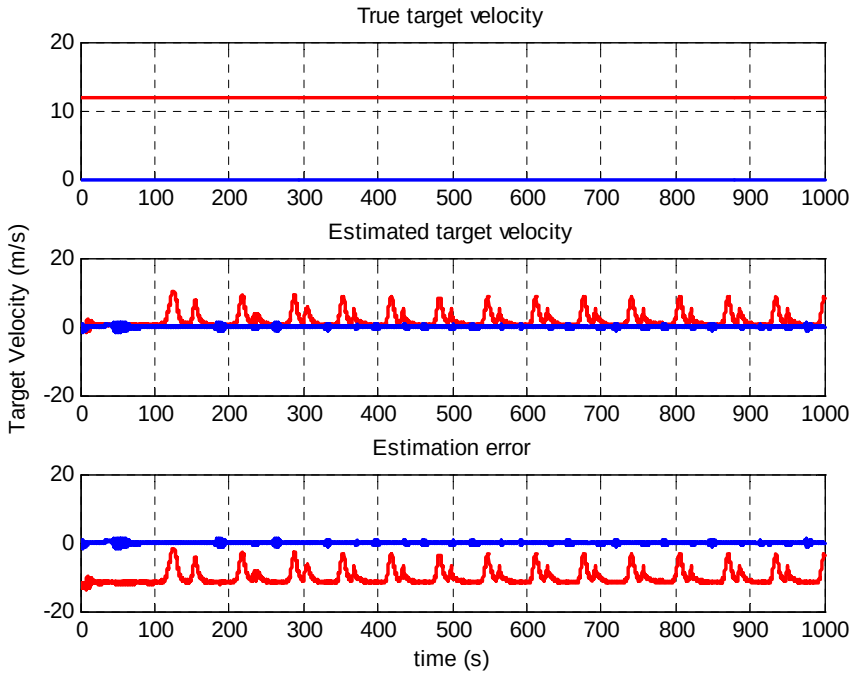

Figure 19. Sensitivity Analysis for $V_t/V_g = 12/25$

Case 5: $V_t/V_g = 14/25$

20(a) SUAV & Target Trajectory

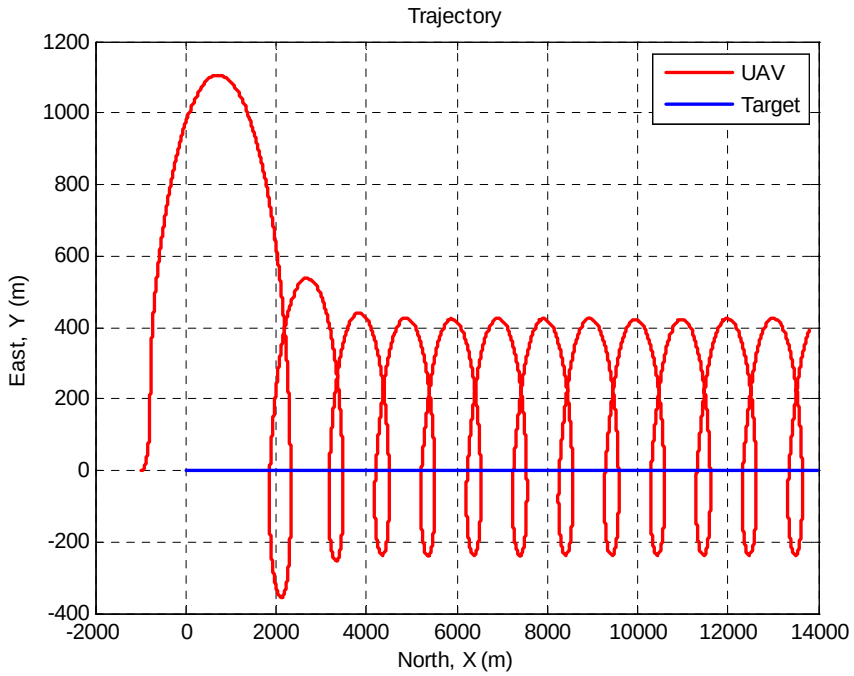

20(b) Range Convergence, Range Holding & Navigation Angle Error Performance

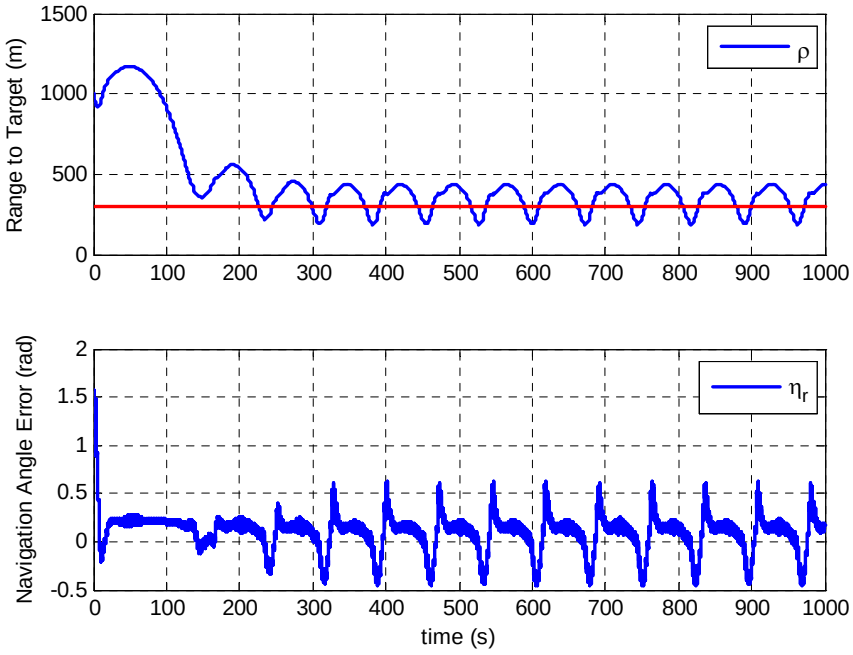

20(c) SUAV Pan & Tilt Errors

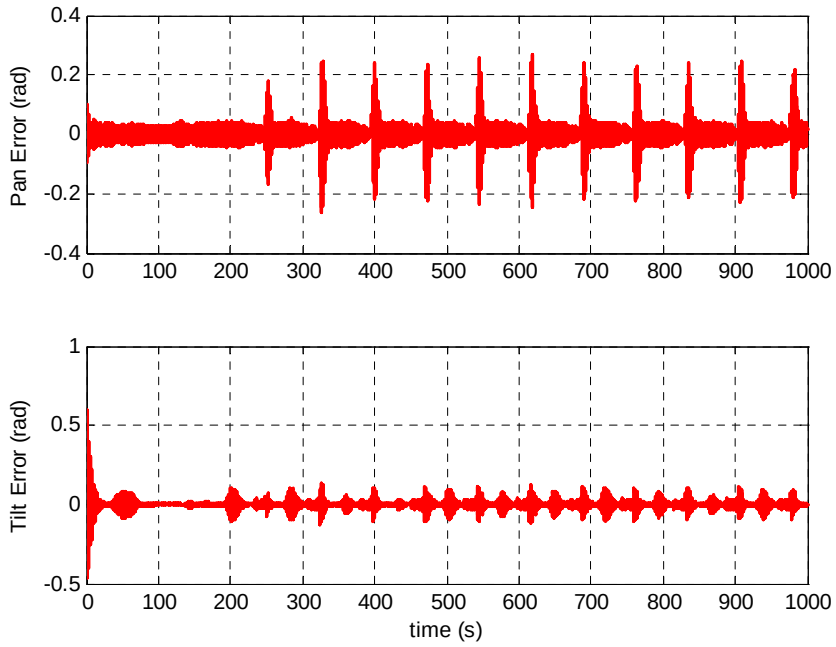

20(d) Target Estimator Performance

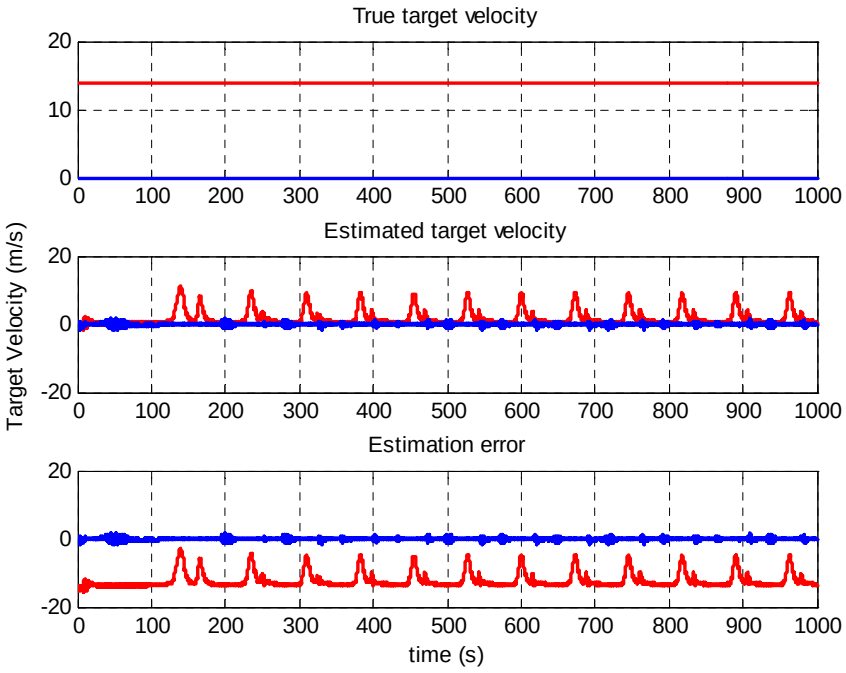

Figure 20. Sensitivity Analysis for $V_t/V_g = 14/25$

D. COMPARISON OF CONTROL LAW'S PERFORMANCE WITH REGARDS TO VARIATIONS IN V_t/V_g

Figure 21 gives a comparison of both control laws with regards to variations in V_t/V_g. For both control laws, it is observed that M_0 increases with increasing V_t/V_g. Thus, both control laws deteriorates in performance when the target velocity is increased. However, the new control law suffers less degradation in performance as compared to the current control law. By regulating $\eta_r(t)$ instead of $\eta(t)$ to 0, the new control law performs better than the current control law in driving the range to target to the commanded range.

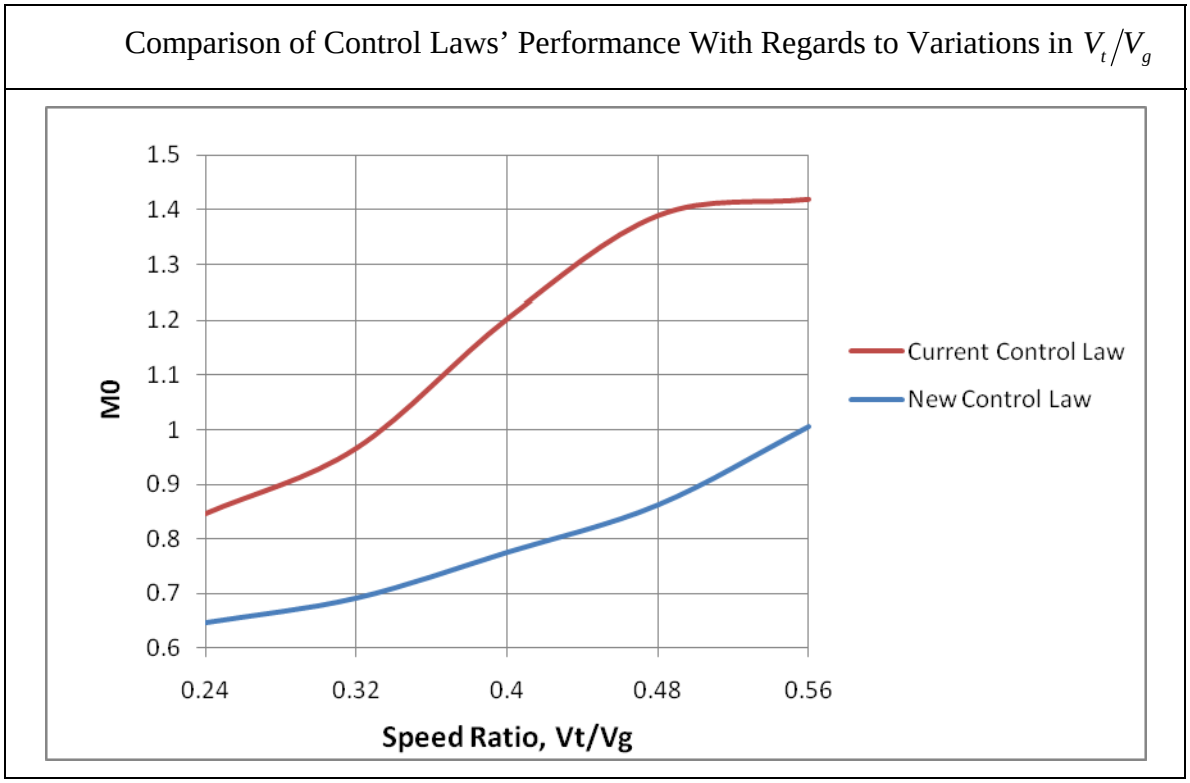

Figure 21. Plot of M_0 vs V_t/V_g for Current and New Control Law

E. SENSITIVITY ANALYSIS OF MOP TO "FREQUENCY OF TLE

The sensitivity analysis of the new control law to "frequency" of TLE is examined in a scenario where the target is moving with a constant heading and the commanded range is 300m. The initial conditions are: (1) SUAV velocity = 25 m/s; (2) Target velocity = 6 m/s; (3) Initial position of the SUAV is at [-1000, 0, 500]; (4) Initial position of the target is at [0, 0, 0] and (5) $k_1 = 0.4$. Thus, the initial horizontal ground range from the SUV to target is 700m.

Performance of M_1, M_2, M_3 and M_0 with Variations to "Frequency" of TLE

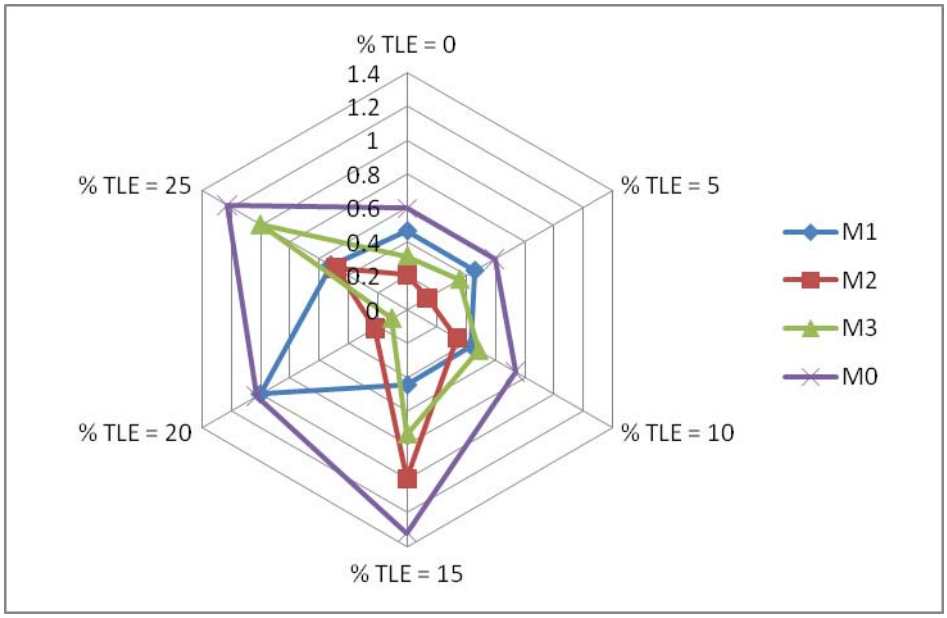

Figure 22. Variation of M_1, M_2, M_3 and M_0 versus "Frequency" of TLE

The following observations can be made from the plot as shown in Figure 22:

(a) It is observed that M_1 decreases with increasing “frequency” of TLE till the “frequency” reaches a value of 10%. Thereafter, M_1 starts to increase with increasing “frequency” of TLE. It is also observed that M_3 increases with increasing “frequency” of TLE. M_2 also increases with increasing “frequency” of TLE till the “frequency” reaches a value of 15%. Thereafter, M_2 starts to decrease with increasing “frequency” of TLE.

(b) From Figure 22, it is observed that M_0 increases with increasing “frequency” of TLE till the “frequency” reaches a value of 15%. Thereafter, the value of M_1 starts to converge to about 1.2 even though the “frequency” of TLE is increasing. When TLE occurs, the camera will not be able to provide an updated target picture to the target estimator. Without the updated target picture, the target estimator will not be able to give a good prediction of the target velocity and heading. As such, the new control law suffers a predictable degradation in performance when TLE occurs.

Figure 23 to 27 presents the detailed results obtained for the new control law when “frequency” of TLE is varied from 5% to 25%.

Case 1: “Frequency” of TLE = 5%

23(a) SUAV & Target Trajectory

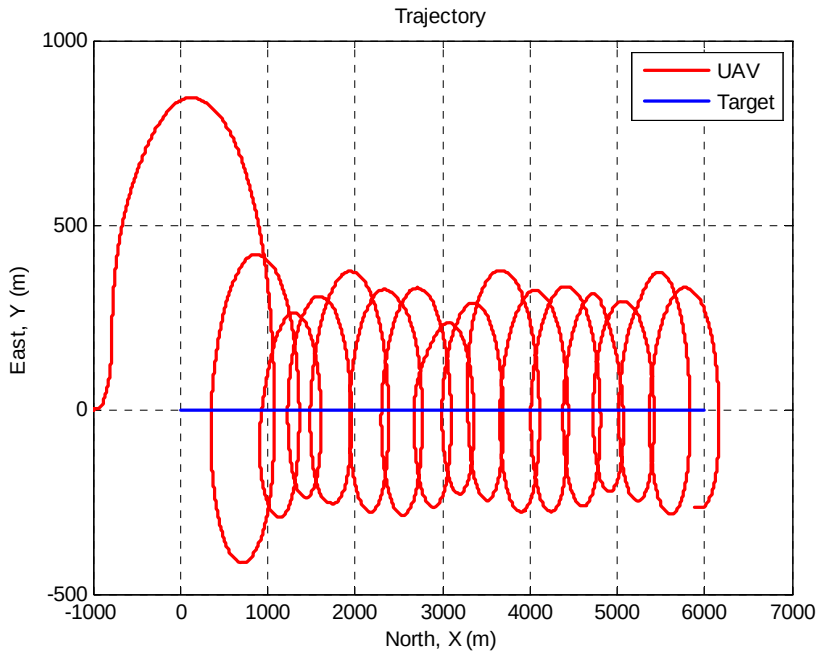

23(b) Range Convergence, Range Holding & Navigation Angle Error Performance

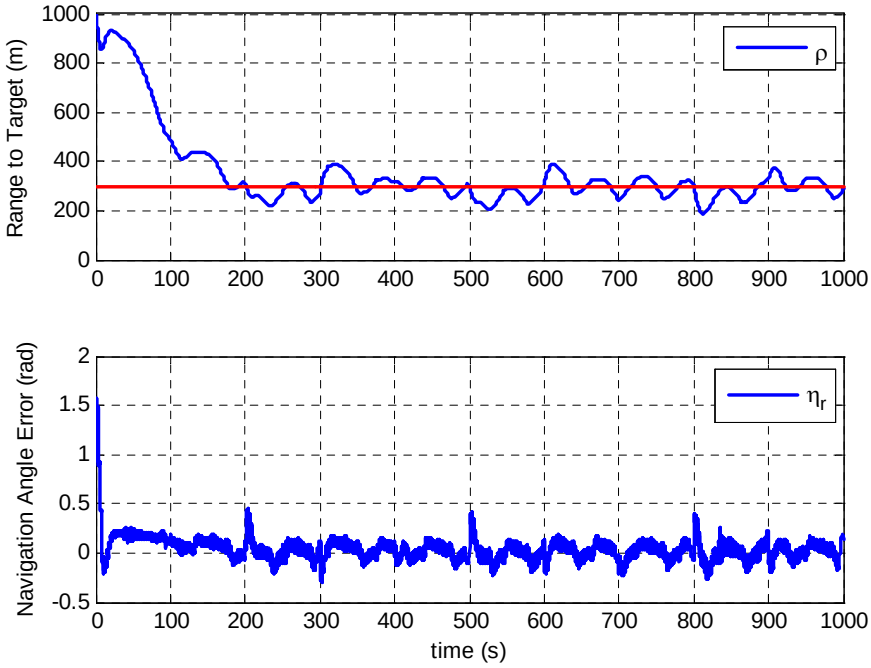

23(c) SUAV Pan & Tilt Errors

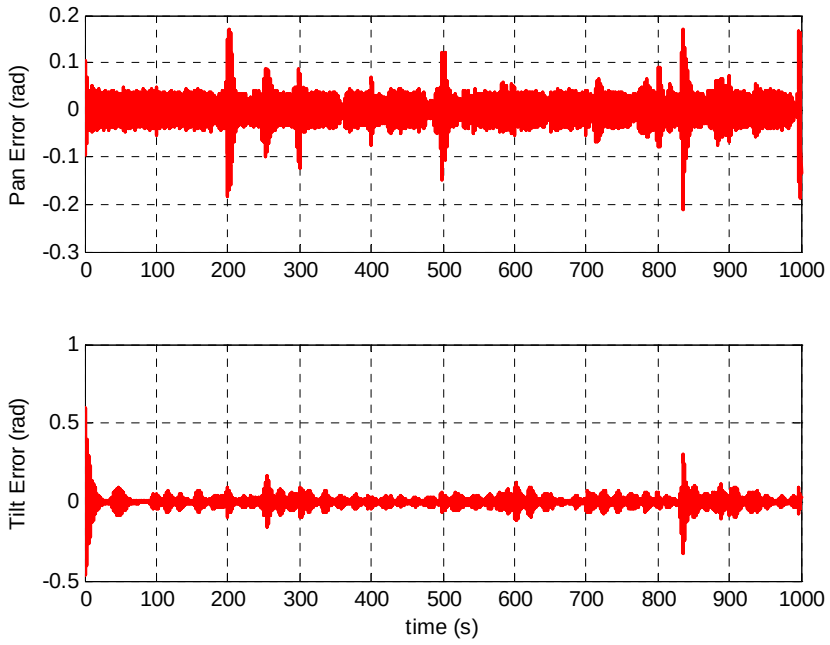

23(d) Target Estimator Performance

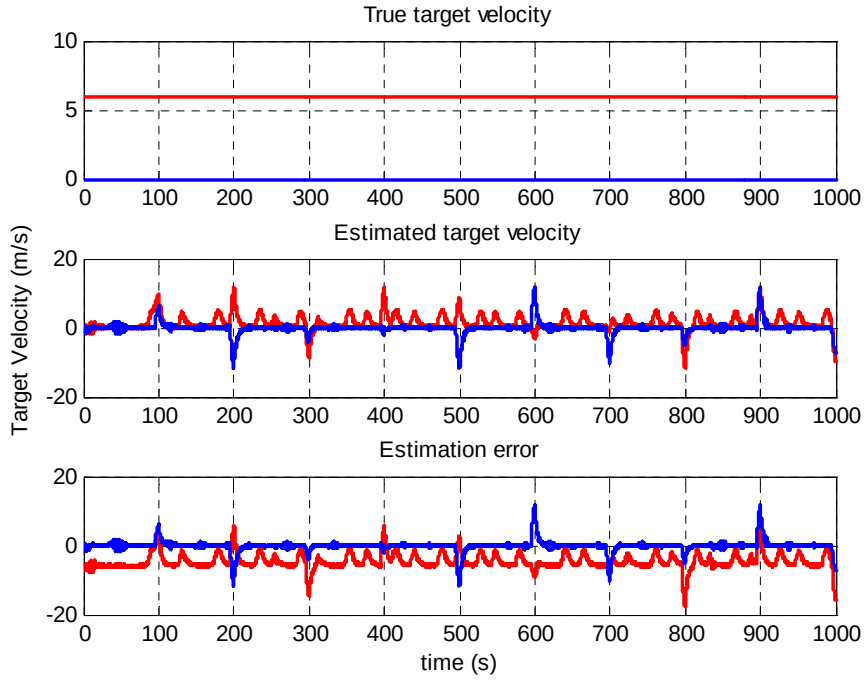

Figure 23. Sensitivity Analysis for "Frequency" of TLE = 5%

Case 2: “Frequency” of TLE = 10%

24(a) SUAV & Target Trajectory

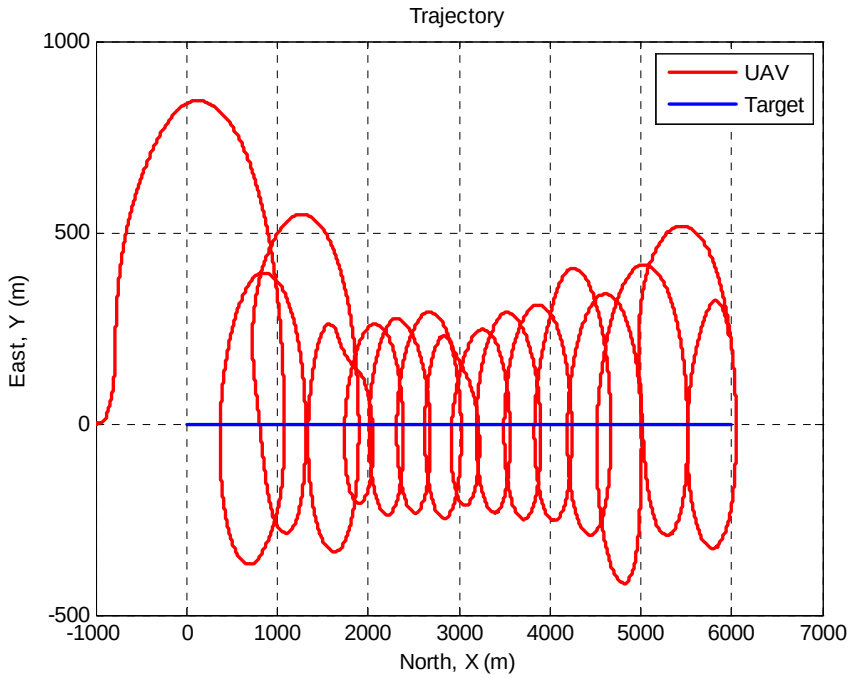

24(b) Range Convergence, Range Holding & Navigation Angle Error Performance

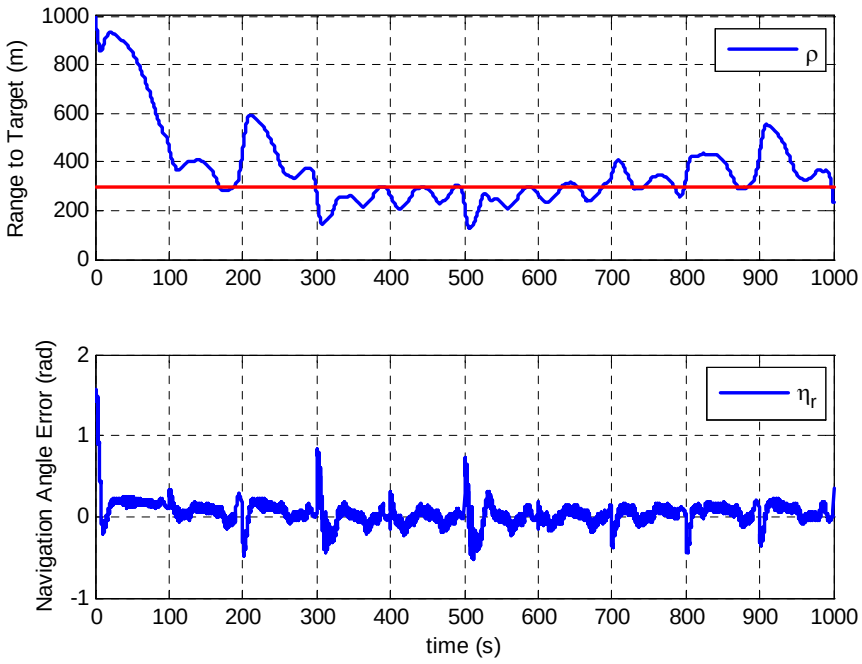

24(c) SUAV Pan & Tilt Errors

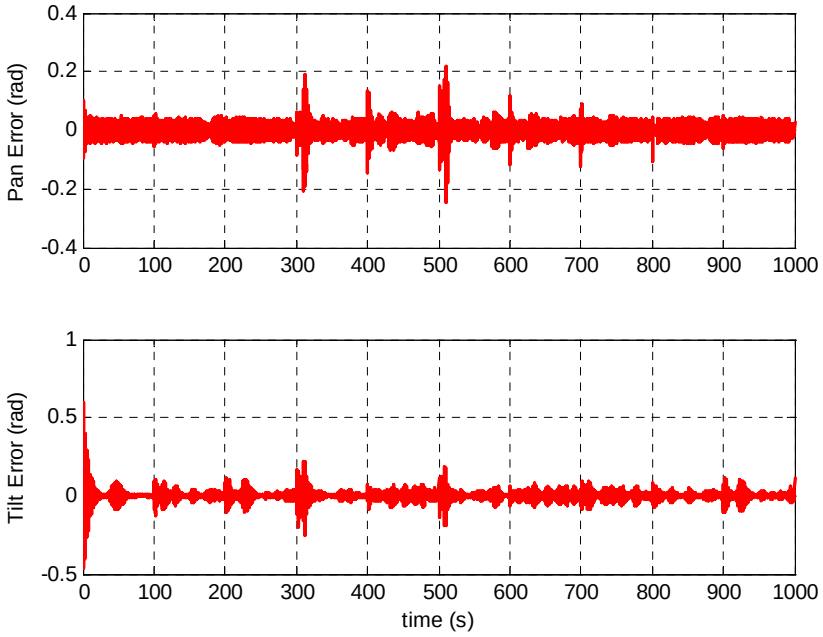

24(d) Target Estimator Performance

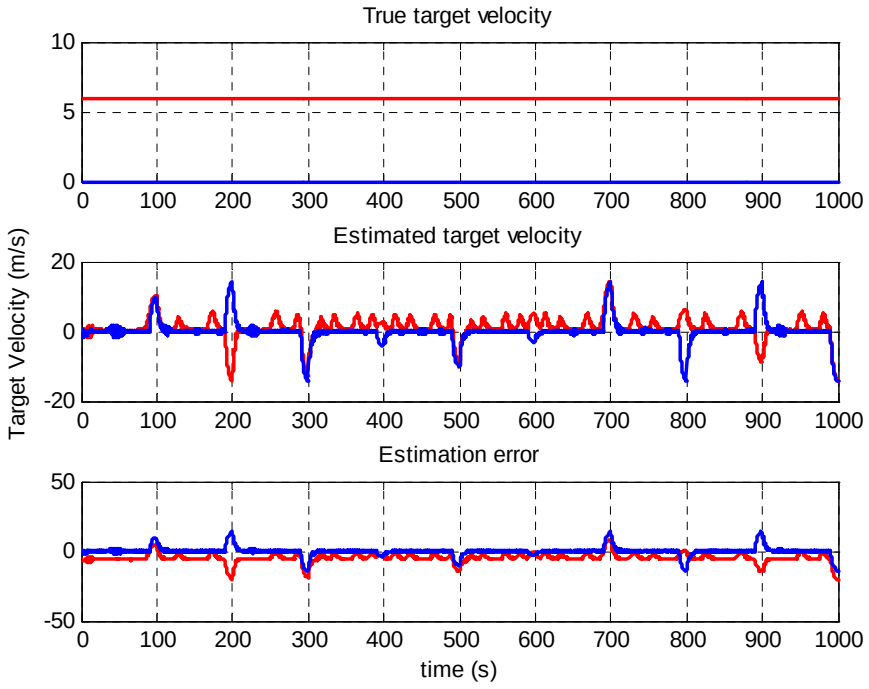

Figure 24. Sensitivity Analysis for "Frequency" of TLE = 10%

Case 3: “Frequency” of TLE = 15%

25(a) SUAV & Target Trajectory

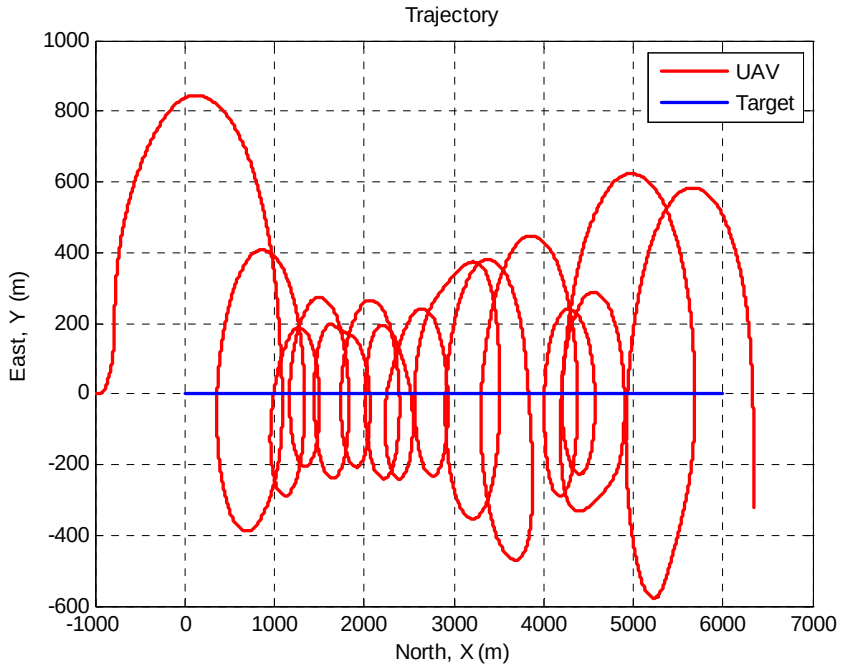

25(b) Range Convergence, Range Holding & Navigation Angle Error Performance

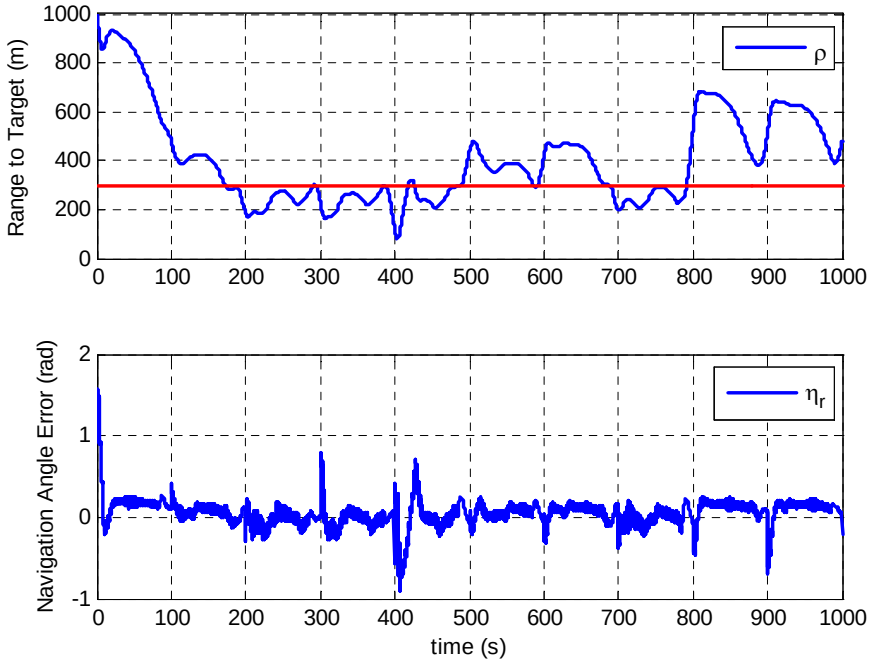

25(c) SUAV Pan & Tilt Errors

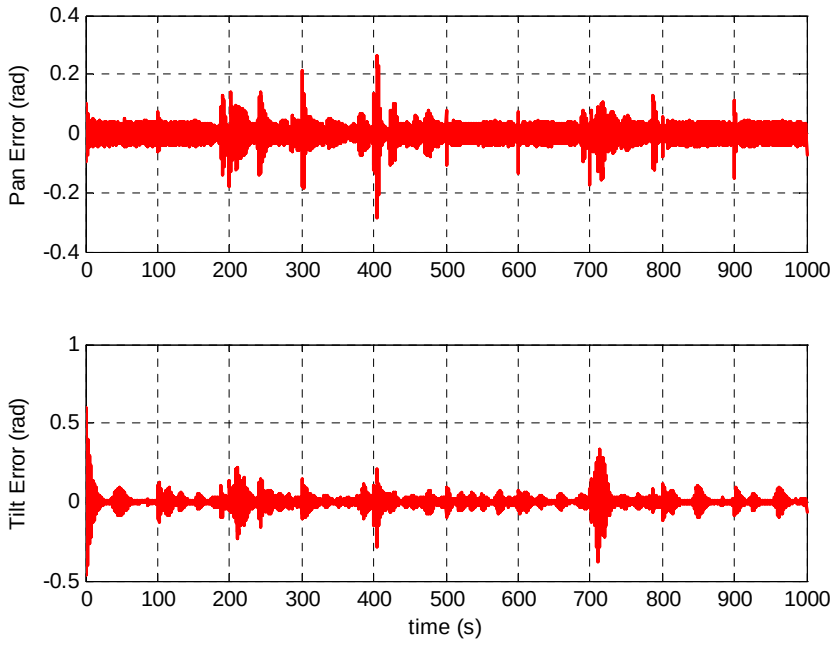

25(d) Target Estimator Performance

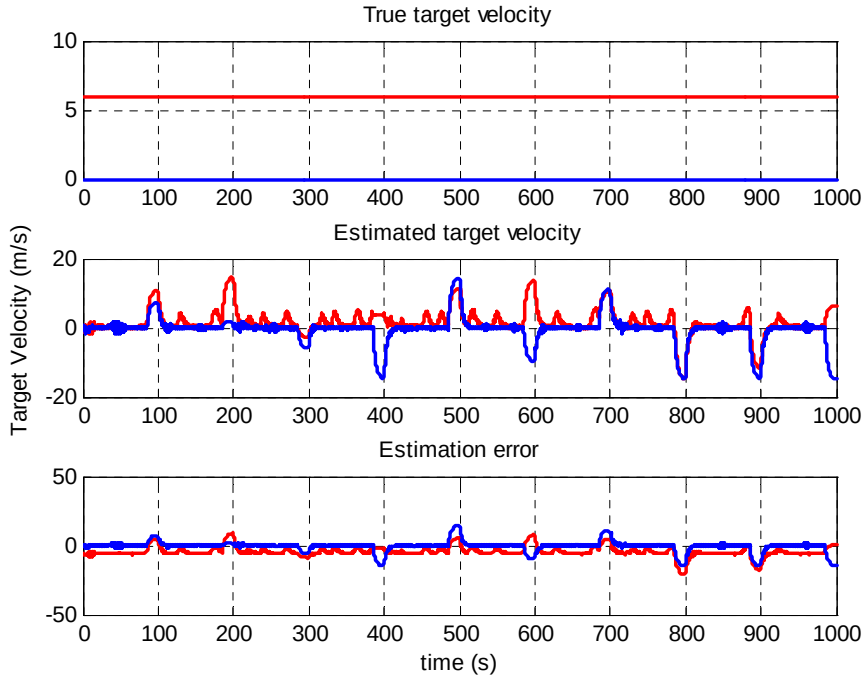

Figure 25. Sensitivity Analysis for “Frequency” of TLE = 15%

Case 4: “Frequency” of TLE = 20%

26(a) SUAV & Target Trajectory

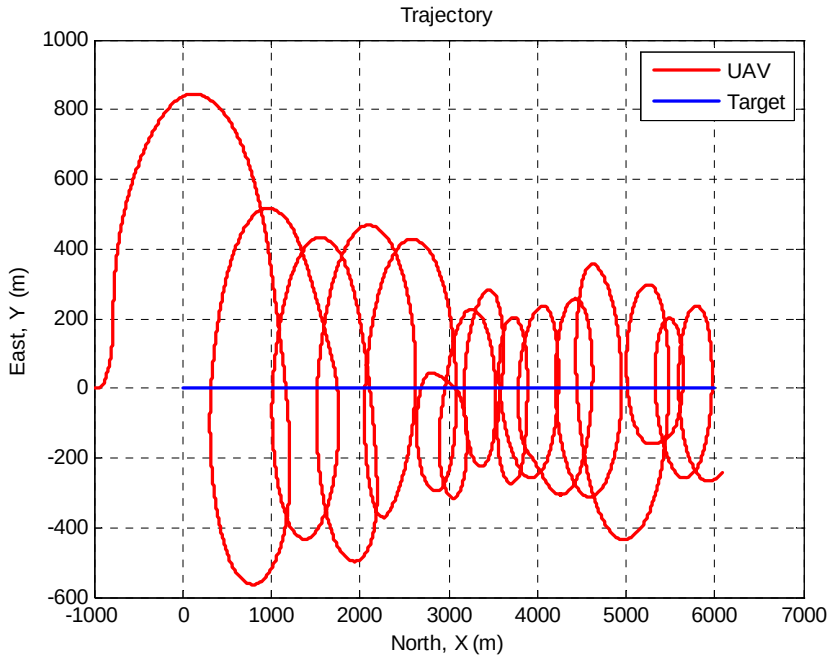

26(b) Range Convergence, Range Holding & Navigation Angle Error Performance

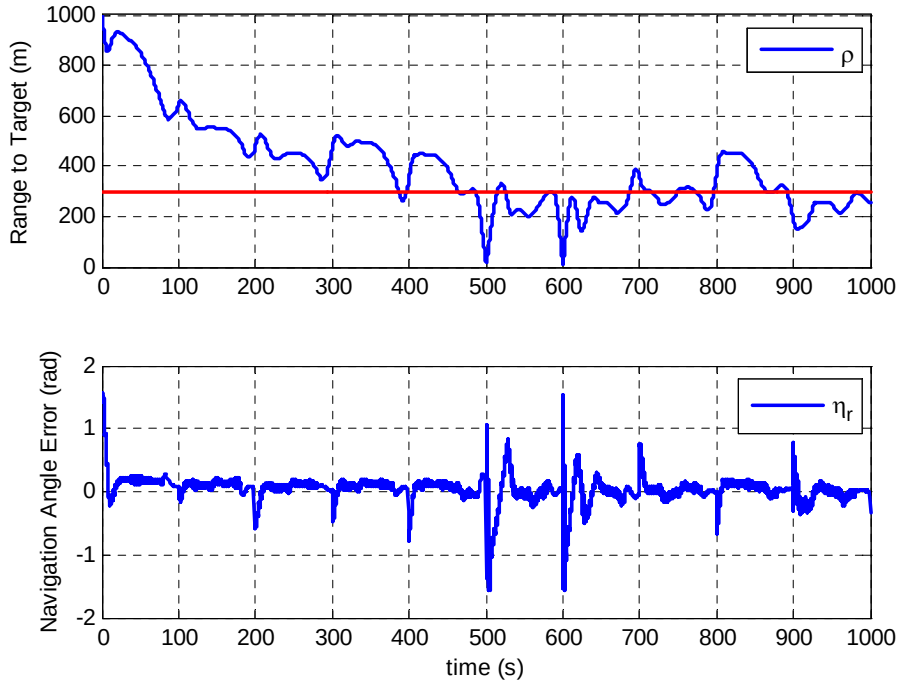

26(c) SUAV Pan & Tilt Errors

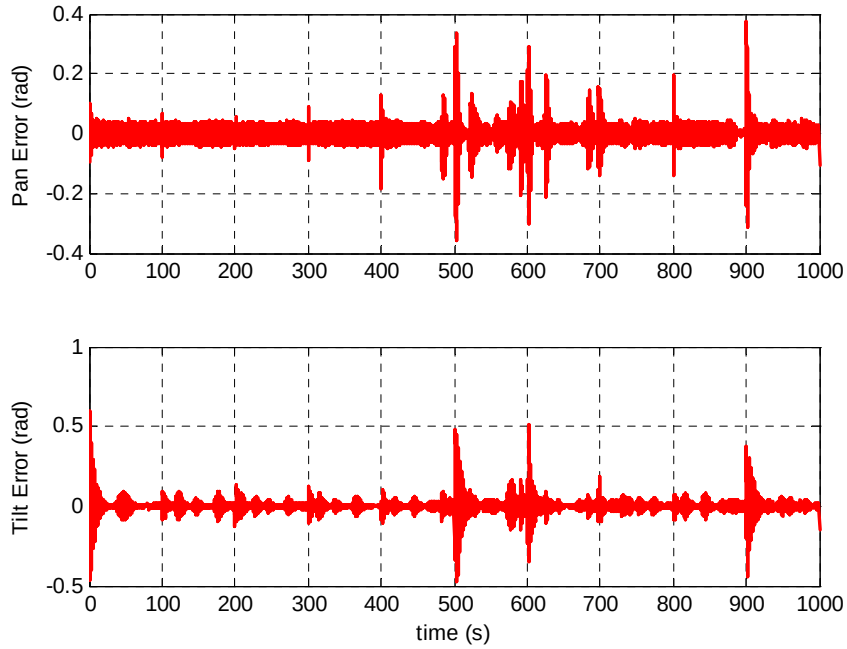

26(d) Target Estimator Performance

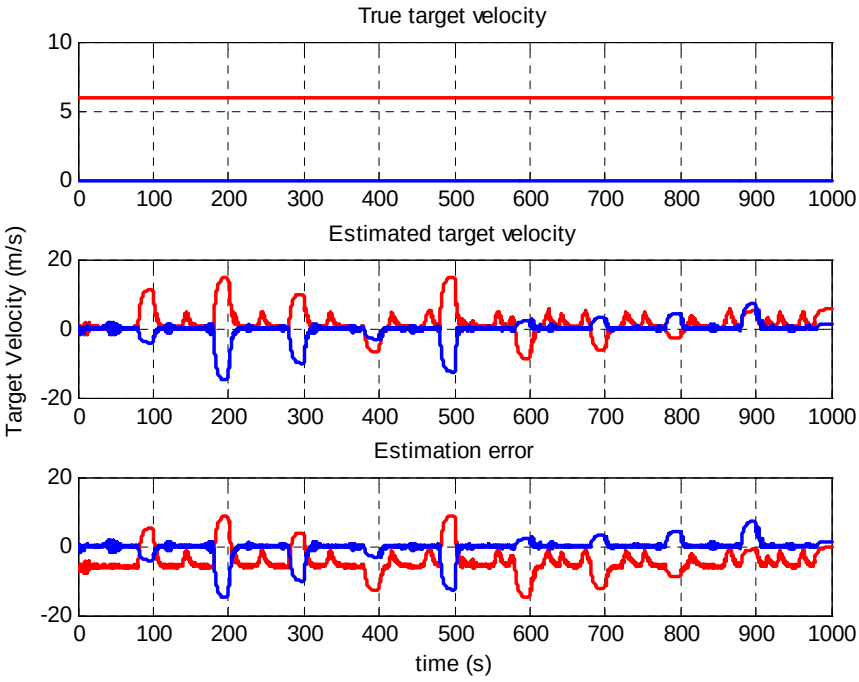

Figure 26. Sensitivity Analysis for "Frequency" of TLE = 20%

Case 5: “Frequency” of TLE = 25%

27(a) SUAV & Target Trajectory

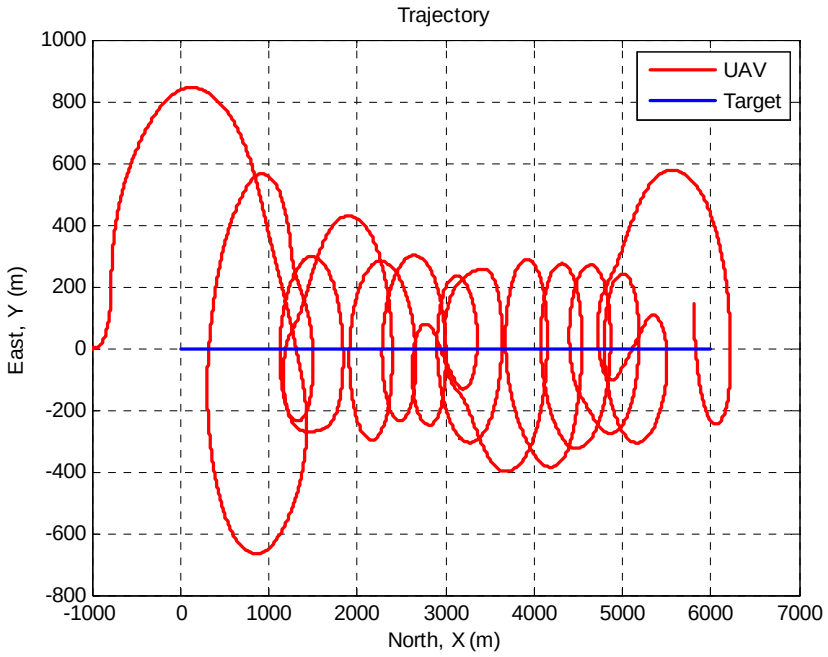

27(b) Range Convergence, Range Holding & Navigation Angle Error Performance

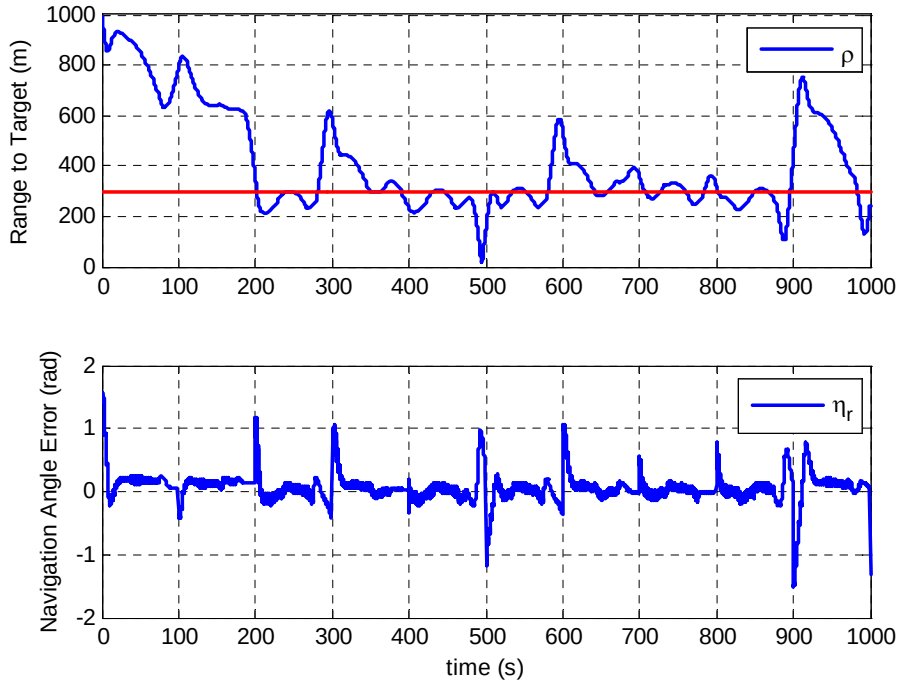

27(c) SUAV Pan & Tilt Errors

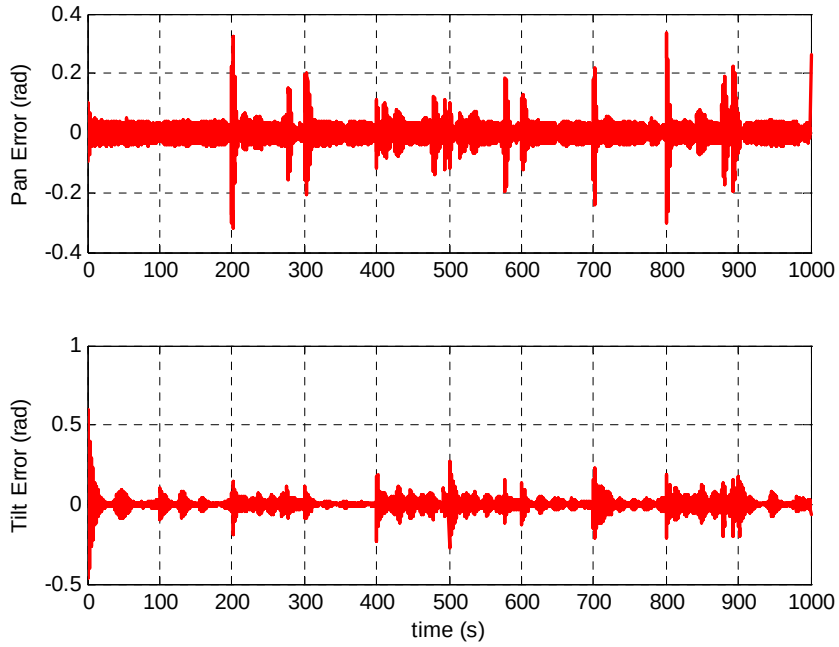

27(d) Target Estimator Performance

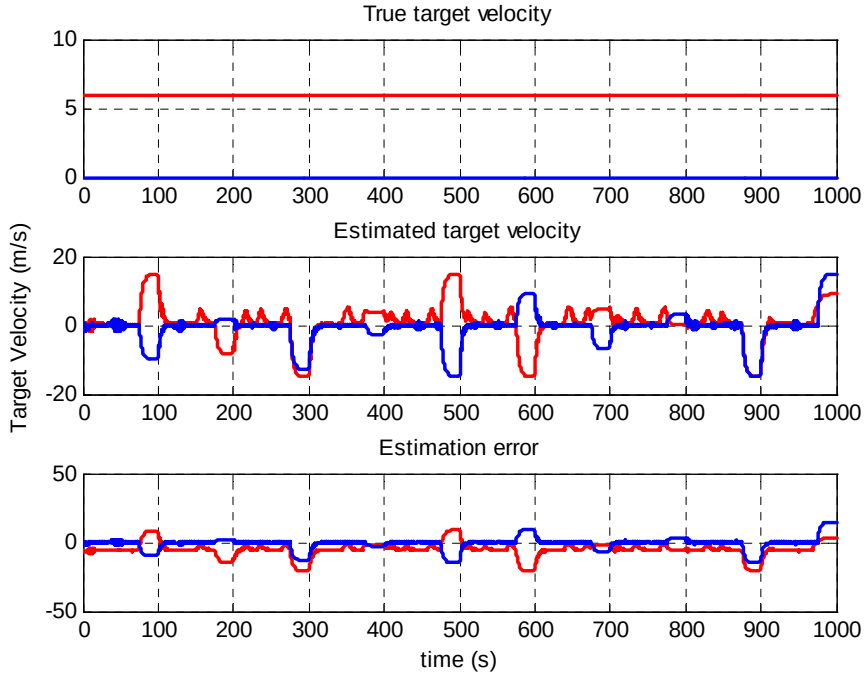

Figure 27. Sensitivity Analysis for “Frequency” of TLE = 25%

F. COMPARISON OF CONTROL LAW'S PERFORMANCE WITH REGARDS TO VARIATIONS IN "FREQUENCY" OF TLE

Figure 28 provides a comparison of both control laws with regards to variations in "frequency" of TLE. For both control laws, it is observed that M_0 increases with increasing "frequency" of TLE. The new control law demonstrates better performance than the current control law when "frequency" of tracking loss events is low (less than 12%). However, as "frequency" of tracking loss events increases (between 12% to 25%), the performance of the new control law degrades more than that of the current control law, as the target estimator is no longer able to provide a good prediction of the target velocity and heading to the control law. Beyond a "frequency" of more than 25%, the value of M_0 appears to converge for both control laws. This suggests the existence of a lower bound in performance for both control laws with regards to variations in "frequency" of TLE.

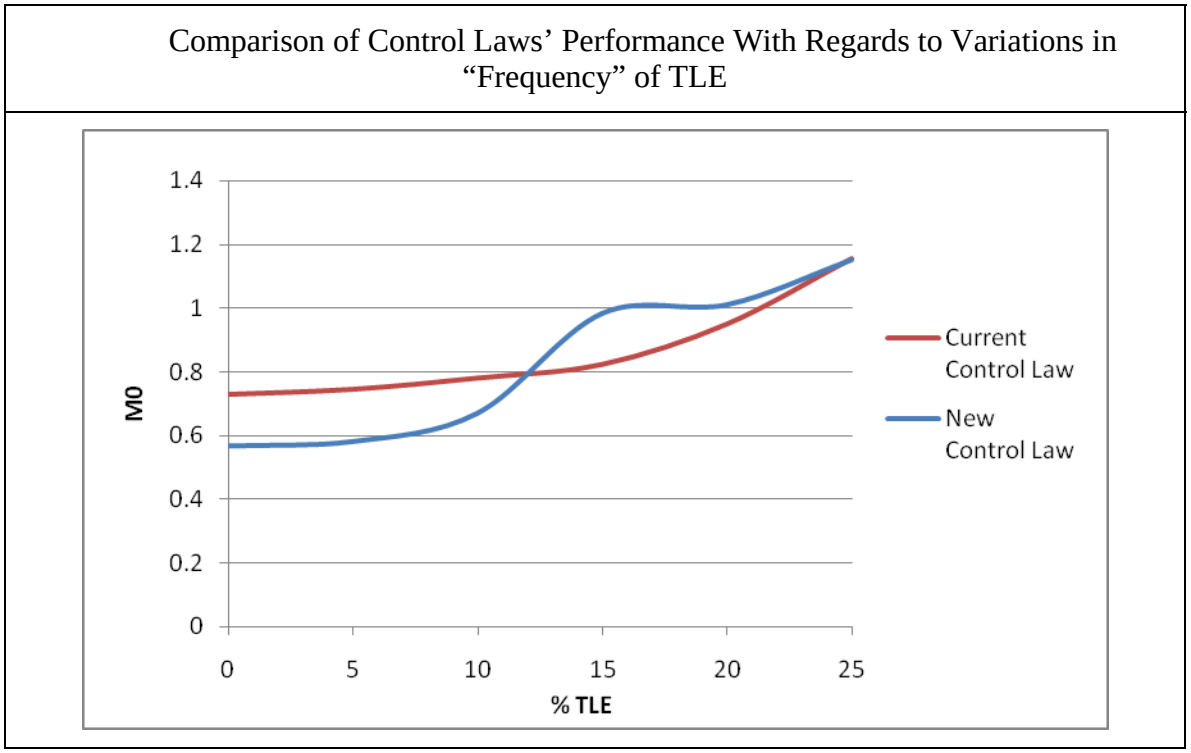

Figure 28. Plot of M_0 vs. "Frequency" of TLE for Current and New Control Law

IV. CONCLUSION AND RECOMMENDATIONS

A. CONCLUSION

To improve the range holding capability and therefore to drive $\dot{\rho}_e$ to zero, a new control objective is formulated by resolving $\vec{V}_g$ and η to the T-frame, whose origin is fixed on the target. As a result, the new control law provides better range holding capability as compared to the previously developed control laws. However, the new control law requires information on target velocity and heading information in order to perform coordinated SUAV guidance and vision based tracking. This additional information is obtained from the newly developed target estimator.

The results obtained from the utilization of the new control law in high fidelity SIMULINK simulation environment are encouraging and comparable to theoretical predictions. The results show that both control laws suffer predictable degradation in performance when subject to the external disturbances and tracking loss events. However, in the absence of tracking loss events, the new control law suffers less degradation in performance as compared to the current control law. When "frequency" of tracking loss events is low (less than 12%), the new control law is still able to provide better performance than the current control law As the "frequency" of tracking loss events increases further (between 12% to 25%), the performance of the new control law starts rapidly degrading converging to that of the initial system; as the target estimator is no longer able to provide a good prediction of the target velocity and heading to the control law.

B. RECOMMENDATIONS

After testing the robustness of the control laws to external disturbances in high fidelity simulation environment, the next logical goal will be to implement the control laws in a hardware-in-the-loop (HIL) simulation before the actual flight test. Although HIL simulation cannot replace actual flight testing, it can help to reduce the likelihood of failure by detecting bugs and deficiencies before risking the hardware in actual flight test.

Moreover, the HIL simulator provides an ideal training tool that can be used in the lab. The HIL simulator had being setup in previous work and the details on the HIL setup can be found in Reference 9 and 10.

LIST OF REFERENCES

[1] D. S. Alberts, J. J. Garstka and F. P. Stein. (1999). "Network Centric Warfare: Developing and Leveraging Information Superiority." Second Edition. *CCRP Publications*. [Accessed November 2009]. Available: http://www.carlisle.army.mil/DIME/documents/Alberts_NCW.pdf

[2] I. H. Wang, V. N. Dobrokhodov, I. I. Kaminer and K. D. Jones. (2005). "On Vision-Based Target Tracking and Range Estimation for Small UAVs." *American Institute of Aeronautics and Astronautics.* [Retrieved August 2009].

[3] V. N. Dobrokhodov, I. I. Kaminer & K. D. Jones and R. Glabcheloo. (2006). "Vision Based Tracking and Motion Estimation for Moving Targets Using Small UAVs." *American Institute of Aeronautics and Astronautics.* [Retrieved August 2009].

[4] L. Ma, C. Cao, N. Hovakimya, V. N. Dobrokhodov and I. I. Kaminer. (2008). "Adaptive Vision-Based Guidance Law with Guaranteed Performance Bounds for Tracking a Ground Target with Time-Varying Velocity." *American Institute of Aeronautics and Astronautics.* [Retrieved August 2009].

[5] Z. Li, V. N. Dobrokhodov, E. Xargay, N. Hovakimyan and I. I. Kaminer. (2009). "Development and Implementation of L_1 Gimbal Tracking Loop Onboard of Small UAV." *American Institute of Aeronautics and Astronautics.* [Retrieved August 2009].

[6] G. M. Siouris. (1993). "Aerospace Avionics Systems: A Modern Synthesis." *New York: Academic Press*.

[7] B. Etkin and L. D. Reid. (1995). "Dynamics of Flight." Third Edition. *New York: John Wiley and Sons*.

[8] R. A. Prince. (2004). "Autonomous Visual Tracking of Stationary Targets Using Small Unmanned Aerial Vehicles." M.S. Thesis. *Naval Postgraduate School, Monterey, CA, U.S.A.*

[9] T. C. Boon. (2006). "Development and Implementation of New Control Law for Visual Based Target Tracking System Onboard Small Unmanned Aerial Vehicles." M.S. Thesis. *Naval Postgraduate School, Monterey, CA, U.S.A.*

[10] M. L. Soh. (2008). "Hardware in the Loop Implementation of Adaptive Vision Based Guidance Law for Ground Target Tracking." M.S. Thesis. *Naval Postgraduate School, Monterey, CA, U.S.A.*

[11] V. N. Dobrokhodov, I. I. Kaminer, K. D. Jones, I. Kitsios, C. Cao, L. Ma, N. Hovakimyan and C. Woolsey. (2007). “Rapid Motion Estimation of a Target Moving with Time-Varying Velocity.” *American Institute of Aeronautics and Astronautics.* [Retrieved August 2009].

[12] C. Cao and N. Hovakimyan. (2008). “Design and Analysis of a Novel L_1 Adaptive Control Architecture with Guaranteed Transient Performance.” *Institute of Electrical and Electronics Engineers.* [Retrieved August 2009].

INITIAL DISTRIBUTION LIST

1. Defense Technical Information Center
   Ft. Belvoir, Virginia

2. Dudley Knox Library
   Naval Postgraduate School
   Monterey, California

3. Professor Issac I. Kaminer
   Naval Postgraduate School
   Monterey, California

4. Professor Vladimir N. Dobrokhodov
   Naval Postgraduate School
   Monterey, California

5. Professor Knox T. Millsaps
   Chairman, Department of Mechanical and Astronautical Engineering
   Naval Postgraduate School
   Monterey, California

6. Professor Yeo Tat Soon
   Director, Temasek Defence Systems Institute
   National University of Singapore
   Singapore

7. Tan Lai Poh (Ms)
   Assistant Manager, Temasek Defence Systems Institute
   National University of Singapore
   Singapore